© 2016. Published by The Company of Biologists Ltd | Development (2016) 143, 1697-1709 doi:10.1242/dev.131318

Regional signals in the planarian body guide stem cell fate in the presence of genomic instability

T. Harshani Peiris[1,2], Daniel Ramirez[1,2], Paul G. Barghouth[1,2], Udokanma Ofoha[1,2], Devon Davidian[1,2], Frank Weckerle[1] and Néstor J. Oviedo[1,2,3,*]

ABSTRACT

Cellular fate decisions are influenced by their topographical location in the adult body. For instance, tissue repair and neoplastic growth are greater in anterior than in posterior regions of adult animals. However, the molecular underpinnings of these regional differences are unknown. We identified a regional switch in the adult planarian body upon systemic disruption of homologous recombination with RNA-interference of *Rad51*. *Rad51* knockdown increases DNA double-strand breaks (DSBs) throughout the body, but stem cells react differently depending on their location along the anteroposterior axis. In the presence of extensive DSBs, cells in the anterior part of the body resist death, whereas cells in the posterior region undergo apoptosis. Furthermore, we found that proliferation of cells with DNA damage is induced in the presence of brain tissue and that the retinoblastoma pathway enables overproliferation of cells with DSBs while attending to the demands of tissue growth and repair. Our results implicate both autonomous and non-autonomous mechanisms as key mediators of regional cell behavior and cellular transformation in the adult body.

KEY WORDS: Stem cells, DNA damage, Planarian, Neoblast, Rad51

INTRODUCTION

The proliferative response of normal and neoplastic cells is influenced by their topographical location along the anteroposterior axis (Auerbach and Auerbach, 1982). In mice, cellular proliferation and engraftment responses are superior in the anterior region of the body (i.e. head and thoracic cavity) to those in posterior areas (Auerbach and Auerbach, 1982; Kobayashi, 1977). Likewise, the effects of carcinogens and the growth of transplanted tumor cells are more aggressive in the anterior than in the posterior regions (Auerbach and Auerbach, 1982; Auerbach et al., 1978; Dispersio, 1981; Kubai and Auerbach, 1980). In humans, survival rates of cutaneous melanoma are attributed to location, with head and neck melanomas presenting the poorest outcomes relative to melanomas in other parts of the body (Lachiewicz et al., 2008; Tseng and Martinez, 2011). Despite these clear observations, the mechanisms underlying regional differences in the growth of normal and neoplastic cells in the adult body are unknown.

Planarians allow for the analysis of cell proliferation during tissue renewal and in response to stress and/or injury in the whole adult organism, providing a paradigm to further study regional regulation of cell proliferation in the adult body. Similar to mice and humans, regional differences in cellular proliferation also exist in the planarian flatworm (Baguñà, 1976; Brøndsted, 1969; Oviedo and Levin, 2007). The neoblast, or planarian stem cell, is the only cell with proliferative capacity within the entire organism, which continuously divides to support the renewal and repair of adult tissues. Uninjured planarians contain larger pools of dividing neoblasts in the anterior region than in the posterior; additionally, regeneration of the head occurs faster than the tail (Baguñà, 1976; Brøndsted, 1969; Oviedo and Levin, 2007; Oviedo et al., 2010). Interestingly, disruption of the tumor suppressor PTEN triggers neoblast hyperproliferation and tissue colonization by abnormal cells. These abnormally proliferative cells are first noted in the anterior part of the planarian (Oviedo et al., 2008c). These results suggest that regional signals along the planarian anteroposterior axis might influence the neoblast's decision to proliferate during cellular turnover, injury repair and cellular transformation.

DNA replication stress is one of the earliest manifestations of cellular transformation (Bartkova et al., 2006; Halazonetis et al., 2008; Macheret and Halazonetis, 2015). Furthermore, DNA damage response, particularly the repair of DNA double-strand breaks (DSBs), serves as an early anti-cancer barrier (Bartkova et al., 2006). Investigating the role of DNA repair mechanisms as key effectors of cell fate along the anteroposterior axis might provide molecular insights about regional regulation of neoblast proliferation. The Rad51 protein is an essential component for homologous recombination, genomic stability and repair of DSBs (Klein, 2008). We identified that systemic disruption of Rad51 via RNA-interference (RNAi) increases DSBs throughout the whole planarian. Strikingly, the cellular response to DSBs depended on the topographical location along the anteroposterior axis. In the presence of DSBs, cells in the anterior region resisted cell death, whereas cells in the posterior underwent apoptosis. We further discovered that this asymmetric topographical response might be established by cues derived from the central nervous system and the retinoblastoma pathway, enabling the survival and proliferation of cells with DSBs in the anterior region of the organism. These experiments reveal newly discovered regulators of cell fate decisions in the adult body and suggest that regional signals modulate tumor suppressor genes during adult tissue renewal. Our data indicate that both cellular location along the anteroposterior axis (non-cell autonomous) and intrinsic cellular properties (cell-autonomous) modulate fate choices in the presence of DNA damage.

RESULTS AND DISCUSSION

Smed-Rad51 is ubiquitously expressed and is essential to maintain DNA integrity

The planarian homolog of *Rad51-A* (*Smed-Rad51*) is expressed throughout the body and is strongly downregulated by lethal doses

[1]Department of Molecular and Cell Biology, School of Natural Sciences, University of California, Merced, CA 95343, USA. [2]Quantitative and Systems Biology Graduate Program, University of California, Merced, CA 95343, USA. [3]Health Sciences Research Institute, University of California, Merced, CA 95343, USA.

*Author for correspondence (noviedo2@ucmerced.edu)

N.J.O., 0000-0002-0213-9781

Received 26 September 2015; Accepted 10 March 2016

Development (2016) 143, 1697-1709 doi:10.1242/dev.131318

of γ-irradiation (Onal et al., 2012; Solana et al., 2012). To discern endogenous topographical differences in *Smed-Rad51* expression, we began by analyzing FACS-isolated cell populations extracted from both the anterior and posterior regions of the body and confirmed *Smed-Rad51* is widely expressed along the anteroposterior axis. Our analysis of FACS-sorted cells revealed that proliferating, irradiation-sensitive neoblasts (X1 cells) express increased levels of *Smed-Rad51* mRNA compared to both early postmitotic (X2 cells) and differentiated cell (Xins) populations (Fig. 1A). The enrichment of Rad51 expression in neoblasts is consistent with its functions during meiosis and germ cells across planarian species (Chinone and Matsumoto, 2014; Xiang et al., 2014). Nonetheless, the role of Rad51 signaling during cellular turnover and repair of adult tissues, which largely relies on the mitotic activity of somatic stem cells, still requires further investigation. This gap in knowledge might be attributed to the fact that homozygous *Rad51* mutations lead to early embryonic lethality and non-viable embryonic stem cells in mice (Lim and Hasty, 1996; Tsuzuki et al., 1996).

To assess the possible roles of Rad51 during cellular turnover, we functionally disrupted *Smed-Rad51* via RNAi [*Rad51(RNAi)*]. This analysis revealed that systemic inhibition of Rad51 leads to a fully penetrant phenotype (100/100 animals) characterized by the progressive loss of tissue in the posterior region and lethality >40 days post-RNAi treatment (Fig. 1B and data not shown). The specific loss of the posterior tissue is an uncommon RNAi phenotype in planarians, thus we assessed whether the efficiency of our RNAi protocol was limited or restricted to a particular region of the animal. Tissues from both the anterior and posterior regions were processed separately to evaluate *Smed-Rad51* mRNA expression and whole animal protein extracts were obtained to assess protein levels after 35 days of *Rad51(RNAi)* treatment. These experiments revealed that after 35 days, the RNAi protocol dramatically reduced Rad51 gene and protein expression throughout the whole animal (Fig. 1C,D). Additionally, we utilized different strategies to functionally downregulate *Smed-Rad51* with double-stranded-RNA (dsRNA) incorporated by feeding (Rouhana et al., 2013) or microinjections specifically

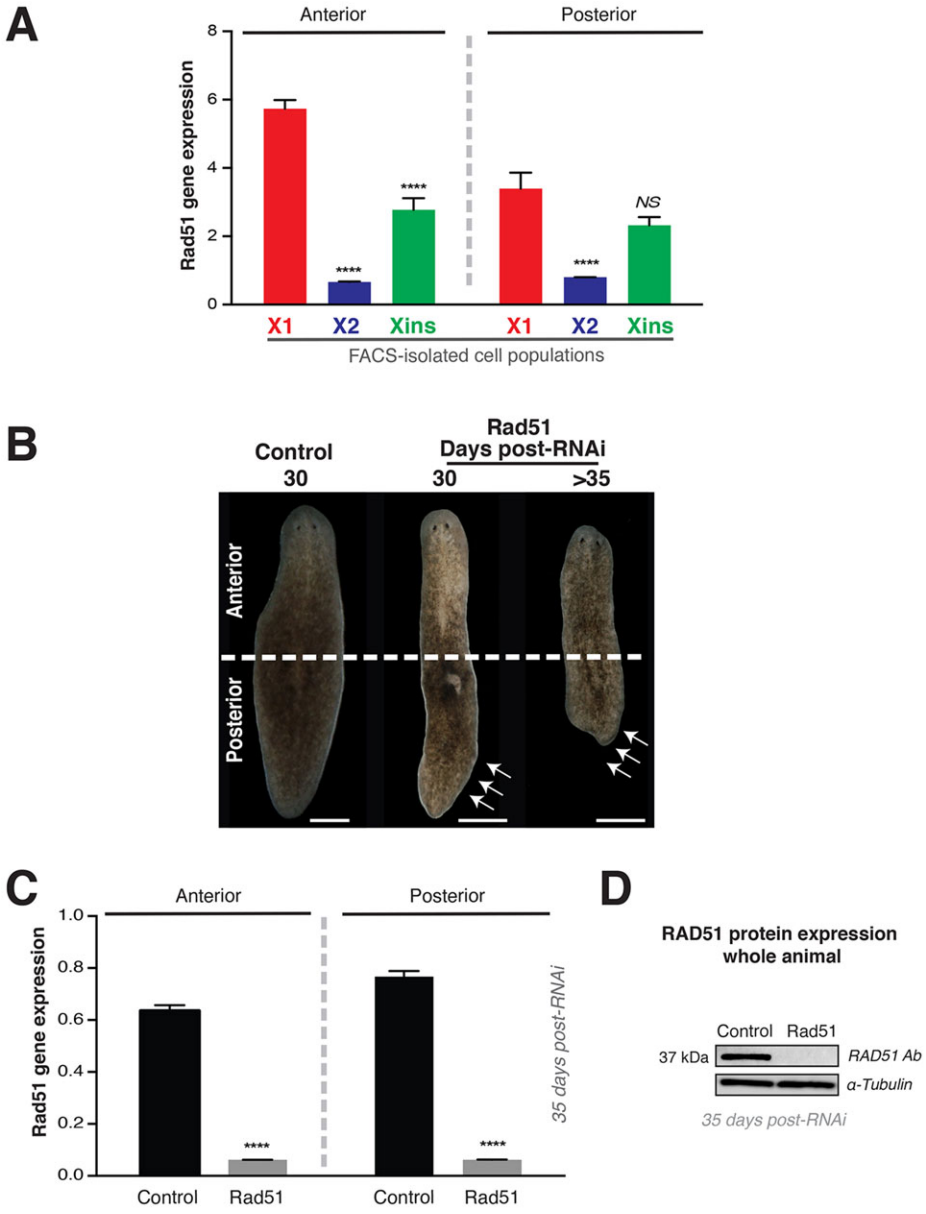

Fig. 1. Rad51 is expressed in neoblasts and differentiated cells and its expression can be downregulated throughout the body. (A) *Smed-Rad51* gene expression levels in FACS-isolated cells (X1, X2 and Xins) measured by qPCR. (B) Representative images of control and *Rad51(RNAi)* animals. The progressive deterioration and tissue lost from posterior body parts are indicated with arrows. (C) *Rad51(RNAi)* reduces expression of *Smed-Rad51* uniformly throughout the body. (D) SMED-RAD51 protein expression is strongly downregulated in the whole organism by *Rad51(RNAi)*. SMED-RAD51 was detected with anti-human RAD51 antibody and alpha tubulin was used as an internal loading control. In A,C, gene expression values represent mean±s.e.m. of triplicates per experiment of at least two biological replicates, each condition was generated by extracting RNA from $n>10$ animals per experiment. The internal control is the ubiquitously expressed clone *H.55.12e*. ****$P<0.0001$; NS, no significance; Tukey's multiple comparisons test.

Development (2016) 143, 1697-1709 doi:10.1242/dev.131318

targeting the anterior or posterior regions of the animal (Oviedo and Levin, 2007). Consistently, we were able to reduce Rad51 expression throughout the animal, leading to the loss of posterior tissue (Fig. S1; data not shown). These findings imply that the phenotype reflects a specific response upon the abrogation of *Smed-Rad51*.

Smed-Rad51 shares a high level of molecular conservation with its homologous counterpart in mammals (Fig. S2), which is crucial for homologous recombination, genomic stability and repair of DNA DSBs (Klein, 2008). To test whether Rad51 is functionally conserved in planarians, we performed *Rad51(RNAi)* treatment and assessed both DNA stability in cells using the Comet assay and chromosomal integrity via karyotyping (Fig. 2A,B). The Comet assay was optimized to detect DSBs and a standard scale was built by using sub-lethal doses of γ-irradiation (1200 rad), which are known to induce DNA damage that is repaired over time (Fig. S3). The RNAi studies revealed that *Smed-Rad51* is essential in maintaining both DNA and chromosomal integrity throughout the whole animal (Fig. 2A,B). Systemic DNA abnormalities in *Rad51 (RNAi)* animals are consistent with the functional conservation of Rad51 in planarians and its distribution along the anteroposterior axis.

To further investigate the function of *Smed-Rad51* in DNA repair, we exposed whole planarians to a single sub-lethal dose of γ-irradiation (1200 rad) that caused DSBs and transiently abrogated neoblast division (Wagner et al., 2011). Specifically, two aspects were analyzed; Rad51 gene and protein levels, and cytoplasmic versus nuclear localization of SMED-RAD51 after γ-irradiation. Both gene and protein expression were downregulated during the first three days post-irradiation, consistent with the disappearance of mitotic activity. Expression peaked at day five and then returned to pre-irradiation levels by day seven. This behavior coincided with the recovery of mitotic activity (Fig. 2C,D and data not shown). Furthermore, analysis of SMED-RAD51 expression in dissociated cells from whole planarians showed that Rad51 protein signal switched from the cytoplasm to the nucleus by day five post-irradiation, implying active DNA repair (Fig. 2E,F). These findings are consistent with a recent report suggesting Rad51 plays roles in DSB repair based on changes in expression pattern during meiosis and after irradiation (Xiang et al., 2014).

Smed-Rad51 is required for proper regulation of cell proliferation and cell death during cellular turnover

The process of cellular turnover depends on a specific balance between cell proliferation and cell death. Thus, we assessed the effects of *Rad51(RNAi)* on cell division and cell death in the adult planarian body that continually undergoes cellular turnover. *Rad51 (RNAi)* reduces neoblast mitotic activity throughout the body. However, this reduction is more pronounced in the posterior area of the planarian, compared with the anterior region in which some cells still divide (Fig. 3A,B; Fig. S1). Intriguingly, suppression of mitosis was accompanied by massive cell death and tissue loss in the posterior area, indicating that it is possible to induce selective elimination of cells and tissues depending on their location along the anteroposterior axis (Fig. 3C-E).

The systemic effects of *Smed-Rad51* downregulation with RNAi are characterized by a dramatic decrease in cell division and a regional specific increase of cell death in the posterior area of the planarian (Fig. 3A-E). To gain insights on the mechanisms regulating cellular decisions upon *Rad51(RNAi)* treatment, we analyzed cells from both the anterior and posterior areas by flow cytometry (Hayashi et al., 2006; Peiris et al., 2016). We found that *Rad51(RNAi)* leads to a ∼50% systemic reduction in the number of proliferative cells (e.g. X1 subpopulation, Fig. S4A). This finding is consistent with a restricted number of cells transitioning into the G2/M phase of the cell cycle (Fig. 3A,B). Furthermore, gene expression analysis of *Smed-cyclin B*, which is needed for the progression of neoblasts into the M phase of the cell cycle, revealed a strong downregulation throughout the animal. However, the reduction in gene expression is accentuated in the posterior compared with the anterior region (Fig. 3F,G). Additionally, regional changes in the expression of neoblast markers and the cellular division progeny were also observed after *Rad51(RNAi)* treatment (Fig. S4B,C). These results suggest that despite a severe reduction of neoblasts in *Rad51(RNAi)* animals, the asymmetric distribution of proliferative cells is sustained.

Cell cycle transition between the S and G2/M phases can be visualized throughout the planarian body by double labeling with the thymidine analogue bromodeoxyuridine (BrdU) and anti-histone-3-phosphorylated (H3P) antibody (Newmark and Sanchez Alvarado, 2000). BrdU is incorporated during the S phase, whereas the H3P antibody labels neoblasts in the G2/M phase. After *Rad51 (RNAi)* treatment, BrdU incorporation was severely reduced but the proliferative asymmetry was maintained as demonstrated by the distribution of $BrdU^+$ and $H3P^+$ cells along the anteroposterior axis (Fig. 3H,I; Fig. S5). Quantification of double $BrdU^+$ and $H3P^+$ cells revealed that 60-70% of cells continuing through the cell cycle are positive for both BrdU and H3P, indicating that the remaining cells in *Rad51(RNAi)* animals transition from the S phase to the M phase with similar dynamics to the control group (Fig. 3J). This result implies that regional asymmetry in the progression through the S/G2/M phases of the cell cycle is still preserved despite fewer neoblasts in *Rad51(RNAi)* animals. Additional experiments are required to address the mechanisms influencing regional levels of cell death in the absence of Rad51. Nonetheless, the whole-body Rad51-silencing strategy we applied reveals unappreciated aspects of regional regulation of cell fate in the presence of DNA damage.

Homologous recombination is required to repair DNA after ionizing irradiation and to maintain DNA integrity along the anteroposterior axis

Unrepaired DSBs pose a great risk for cell survival and malignancy. An extensive number of neoblasts and differentiated cells undergo apoptosis in the posterior region, unlike the anterior region (Fig. 3C-E). Nonetheless, the presence of cell division in *Rad51 (RNAi)* animals suggests that either some cells maintain DNA integrity through a Rad51-independent mechanism, or mitosis occurs despite DNA damage. DSB repair proceeds predominantly through two mechanisms; homologous recombination and Ku-dependent non-homologous end joining (NHEJ) (Lord and Ashworth, 2012). We identified in the *Schmidtea mediterranea* genome components associated with NHEJ such as Ku, MRE11 and ATM (ataxia telangiectasia mutated). RNAi knockout of *Smed-Ku70*, *Smed-MRE11* and *Smed-ATM* reduced neoblast division and was further reduced with simultaneous downregulation of *Smed-Rad51*with *Rad51(RNAi)* (Fig. 4A,B). These results suggest that cell division after *Rad51(RNAi)* proceeds without intervention of the NHEJ DNA repair mechanisms, which is consistent with the levels of DSBs present throughout the experimental group. This also implies that after *Smed-Rad51* knockdown, neoblasts with genomic instability are prone to proliferate, a pervasive feature of tumor cells (Halazonetis et al., 2008).

To further understand the mechanisms planarians use to repair damaged DNA, we tested both the roles of homologous

Development (2016) 143, 1697-1709 doi:10.1242/dev.131318

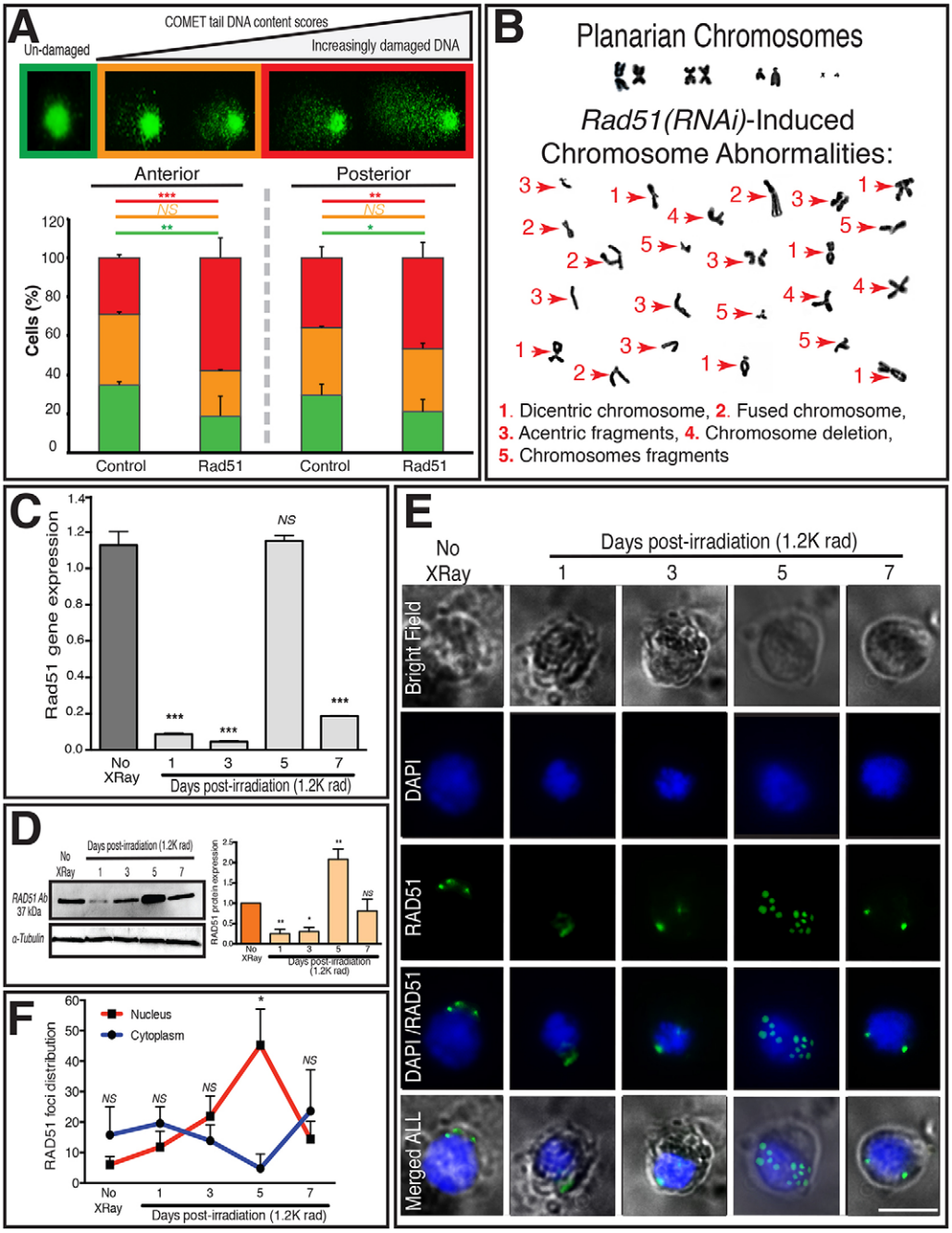

Fig. 2. Rad51 maintains genomic stability and its expression is regulated by gamma irradiation-induced DNA damage. (A) DNA damage in anterior and posterior specific regions were assessed by the Comet assay, gel electrophoresis under alkaline conditions. Visual scoring was used to quantify DNA damage, color-coded key at top represents undamaged (green), moderate damage (orange) and extremely damaged DNA (red) shown in either anterior or posterior regions. (B) Mitotic metaphase spread from whole animals shows multiple chromosome abnormalities after *Rad51(RNAi)*. (C) *Smed-Rad51* mRNA levels from whole animals measured with qPCR over one week post-irradiation. (D) SMED-RAD51 changes after sub-lethal irradiation were measured by western blot using protein extracts from whole animals at each time point. Quantification for each respective time point is shown to the right (bar graph). SMED-RAD51 was detected with anti-human RAD51 antibody and alpha tubulin was used as an internal loading control. (E) Spatial distribution of SMED-RAD51 immunostaining (green) in reference to the cell nucleus (stained with DAPI, blue). Notice SMED-RAD51 signal is mostly perinuclear but at day five after sub-lethal irradiation the signal is closely associated with the cell nucleus. Overlay between bright field and fluorescent images was used to evaluate SMED-RAD51 spatial location (bottom row). The images were obtained from whole animal dissociation. Scale bar: 10 µm. (F) Percentage of SMED-RAD51 foci distribution after sub-lethal irradiation. In A-D,F, analyses were performed using animals ~30 days after first dsRNA injection. Values represent mean±s.e.m. of at least three biological replicates and each condition was generated with 10-20 animals per experiment. **P*<0.01, ***P*<0.005, ****P*<0.0005; NS, not significant; Tukey's multiple comparison test.

recombination and NHEJ after a sub-lethal dose of γ-irradiation (1200 rad). Sub-lethally irradiated *Rad51(RNAi)*-treated animals did not recover cell division and died soon after, whereas RNAi of *Smed-Ku70*, *Smed-MRE11* or *Smed-ATM* and the untreated control group, recovered mitotic activity 7 days post-irradiation (Fig. 4C). Rad51 function is facilitated by the breast cancer type 2 susceptibility protein (BRCA2) (Lord and Ashworth, 2012) and RNAi of its planarian homolog *Smed-BRCA2* (Pearson and Sanchez

Development (2016) 143, 1697-1709 doi:10.1242/dev.131318

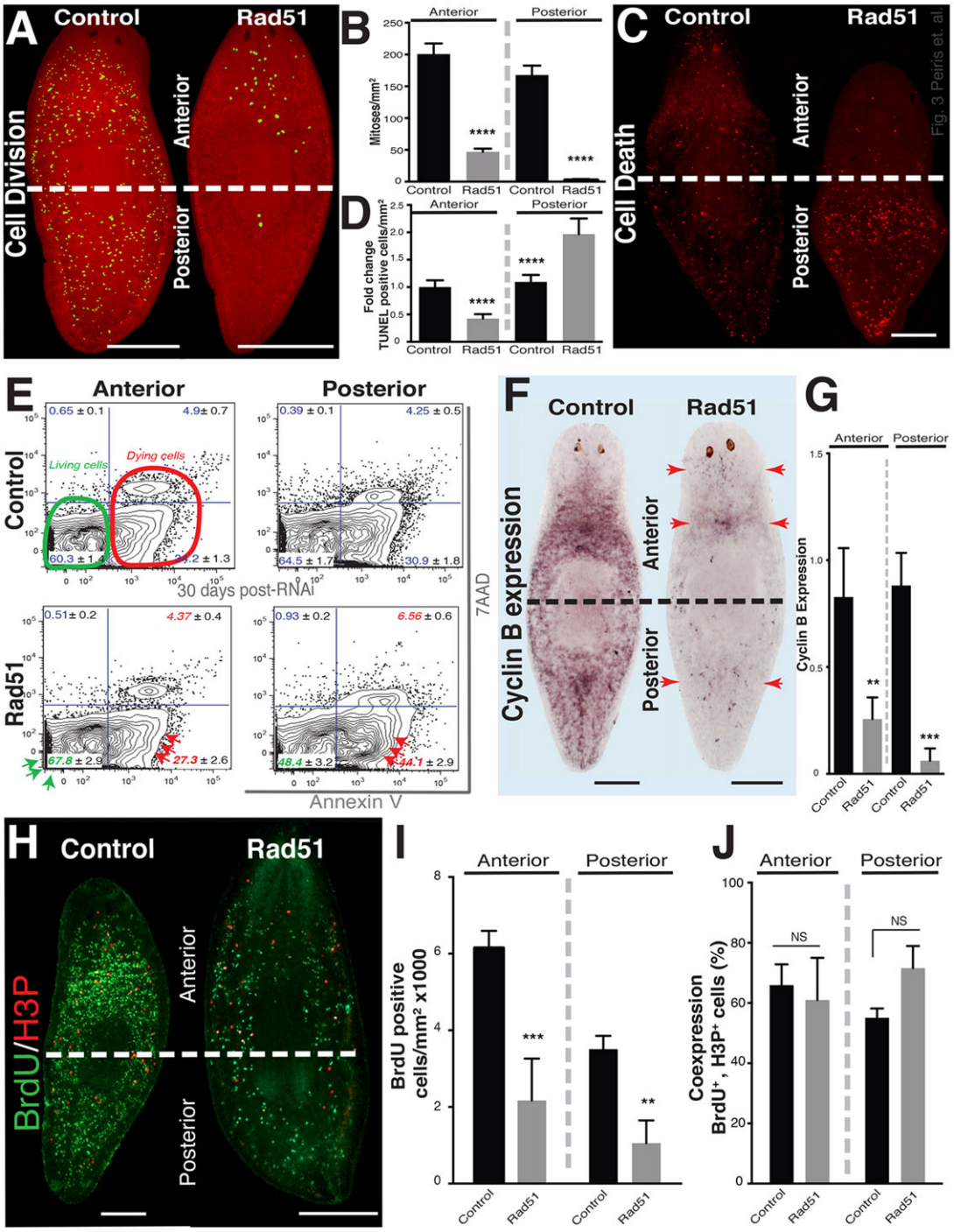

Fig. 3. *Rad51(RNAi)* alters cell proliferation and cell death during systemic cellular turnover in adult planarians. (A) Representative images of mitoses by whole-mount immunostaining with anti-H3P antibody (yellow dots). Dotted line indicates the limits between anterior and posterior areas. (B) Quantification of mitotic cells in the anterior and posterior regions, *n*>25 animals per condition. Cell division disappears over time and animals die after day 40-45 post-*Rad51 (RNAi)* treatment (20 out of 20 animals, data not shown). (C) Whole-mount immunostaining labeling TUNEL-positive nuclei (cell death, red dots) along the anteroposterior axis. (D) Quantification of TUNEL-positive nuclei (cell death levels) in the anterior and posterior regions, *n*>10 animals per condition. (E) The frequency distribution between viable and dead cells visualized with Annexin V and 7 AAD staining in different regions of the animal. Annexin V−/7 AAD− quadrant includes viable cells (outlined green). Annexin V+/7 AAD− and Annexin V+/7 AAD+ indicate cells that are in early and late (necrotic) stages of cell death, respectively (outlined red). The numbers in each quadrant indicate the percentage of cells with that staining profile. (F,G) Expression levels for *Smed-cyclin-B* spatial distribution determined by whole-mount ISH (F) and gene expression levels determined by quantitative PCR (G) in both anterior and posterior regions. Reduction in *Smed-cyclin-B* ISH expression is indicated by red arrows. Gene expression levels are relative to the ubiquitously expressed clone *H.55.12e*. (H) Representative images of whole-mount immunostaining with BrdU and anti-H3P antibody. Green signal corresponds to BrdU incorporated after an 8-10 h pulse, red signal represents cells undergoing mitoses and orange signal represents co-expression in both control and *Rad51(RNAi)* animals. (I) Quantification of cells that incorporated BrdU along the anteroposterior axis. (J) Percentage of cells double-positive (co-expressing) for BrdU and H3P along the anteroposterior axis. In B,D,G,I,J values represent mean±s.e.m. of at least two to three biological replicates and each condition was processed with 10-20 animals per experiment. ***P*<0.005, ****P*<0.0005, *****P*<0.0001; NS, no significance; two-way ANOVA. Scale bars: 200 µm.

Development (2016) 143, 1697-1709 doi:10.1242/dev.131318

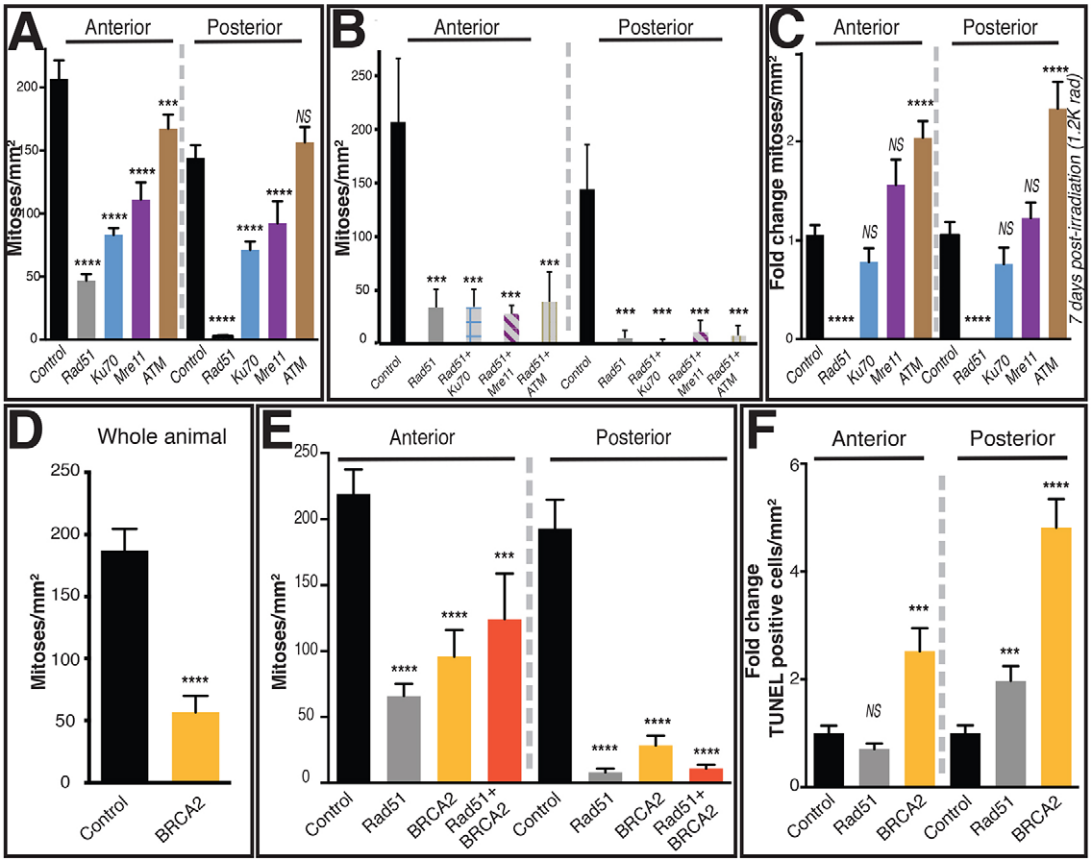

Fig. 4. Homologous recombination and non-homologous end joining (NHEJ) regulate cell division in planarians. (A,B) Levels of mitoses along the anteroposterior axis after individual or simultaneous downregulation of molecules associated with homologous recombination (*Rad51*) and NHEJ (*Ku70*, *Mre11*, *ATM*). (C) Mitotic activity seven days after sublethal doses of gamma irradiation (1200 rad) on animals subjected to downregulation of molecules associated with homologous recombination and NHEJ. Notice *Rad51(RNAi)* sub-lethally irradiated animals fail to recover mitotic activity. (D-F) Mitotic levels after downregulation of BRCA2, a component of homologous recombination, resembles the *Rad51(RNAi)* phenotype, including increased cell death in the posterior region (F). In A-F, all analyses were performed on intact animals ~30 days after first dsRNA and graphs represents mean±s.e.m. of at least two biological replicates with $n>10$ animals in each experiment. ***$P<0.0005$, ****$P<0.0001$; NS, not significant; Tukey's multiple comparison test.

Alvarado, 2010) reproduced the Rad51 phenotype (Fig. 4D,E). This demonstrates both components of the homologous recombination pathway reduce cell proliferation and alter patterns of cell death along the anteroposterior axis (Fig. 4D-F). Taken together, these data suggest that in *S. mediterranea* homologous recombination is the main pathway to: (1) repair DNA after ionizing irradiation and (2) maintain genomic integrity along the anteroposterior axis.

The retinoblastoma pathway mediates cell cycle progression in the presence of DSBs

The anterior region of *Rad51(RNAi)* animals displayed extensive DNA damage and unexpectedly low levels of cell death compared with controls (Figs 2, 3). This is a consistent feature observed in cells with genomic instability that resist undergoing cell death. The establishment and maintenance of cell survival in the presence of DNA damage converge into two pathways controlled by the tumor suppressors p53 and retinoblastoma (Rb) (Campisi, 2005). To assess mechanisms controlling cell fate decisions upon DNA damage, we optimized an RNAi strategy to simultaneously downregulate p53, Rb and Rad51 (Fig. S6), and evaluated cell division along the planarian anteroposterior axis (Fig. 5A,B). In order to downregulate these genes, all of which are required for neoblast maintenance, we developed a dsRNA injection schedule that avoided the depletion of mitotic activity before fixation. Specifically, two variables were considered: (1) the time of mitotic depletion after the first dsRNA injection of each individual gene (i.e.: *Rad51*>40 days; *Rb*>20 days and *p53*>30 days) and (2) the pattern in which mitotic activity vanishes along the anteroposterior axis upon RNAi treatment. For example, mitotic activity progressively diminished from the posterior to the anterior region after injection with *Rad51-RNAi*, whereas *Rb*- and *p53-RNAi*-depleted mitotic activity started in the anterior region, progressing to the posterior region. Therefore, dsRNA injections involving Rb started at day 17 after the initiation of *Rad51(RNAi)* treatment so that by the day of fixation, the Rb phenotype was 13 days after the first injection and still contained dividing cells (Fig. 5A,B).

The tumor suppressor p53 is a crucial downstream component of the DNA damage response (DDR) (Halazonetis et al., 2008). Double RNAi knockdown of p53 and Rad51 resulted in a noticeable increase in mitoses in both anterior and posterior regions when compared with *Rad51(RNAi)* alone. *p53(RNAi)* restricts cell division over time, which is consistent with its role in neoblast maintenance (Pearson and Sanchez Alvarado, 2010). Nonetheless, dividing cells were still present in both the anterior and posterior regions when p53 RNAi knockdown was done individually or combined with knockdown of Rad51 or Rb (Fig. 5A,B). This finding indicates that p53 restricts mitosis in the Rad51 phenotype and confirms that its functions in DDR are

Development (2016) 143, 1697-1709 doi:10.1242/dev.131318

A Percentage of cell division

CONDITION	ANTERIOR	POSTERIOR
Control	100 ± 11.7	100 ± 12.3
Rad51	11.2 ± 4.8***	0.7 ± 0.5 ***
p53	246 ± 25.4****	176.4 ± 27.9**
Rb	25.4 ± 7.2***	82 ± 18.24 NS
p53 + Rb	55.9 ± 9.6**	88.7 ± 5.1 NS
Rad51 + p53	33.2 ± 5.6***	11.9 ± 3.6 ***
Rad51 + Rb	6 ± 3.3****	0.4 ± 0.4 ****
Rad51 + p53 + Rb	3.5 ± 2.3****	1.1 ± 0.7 ****

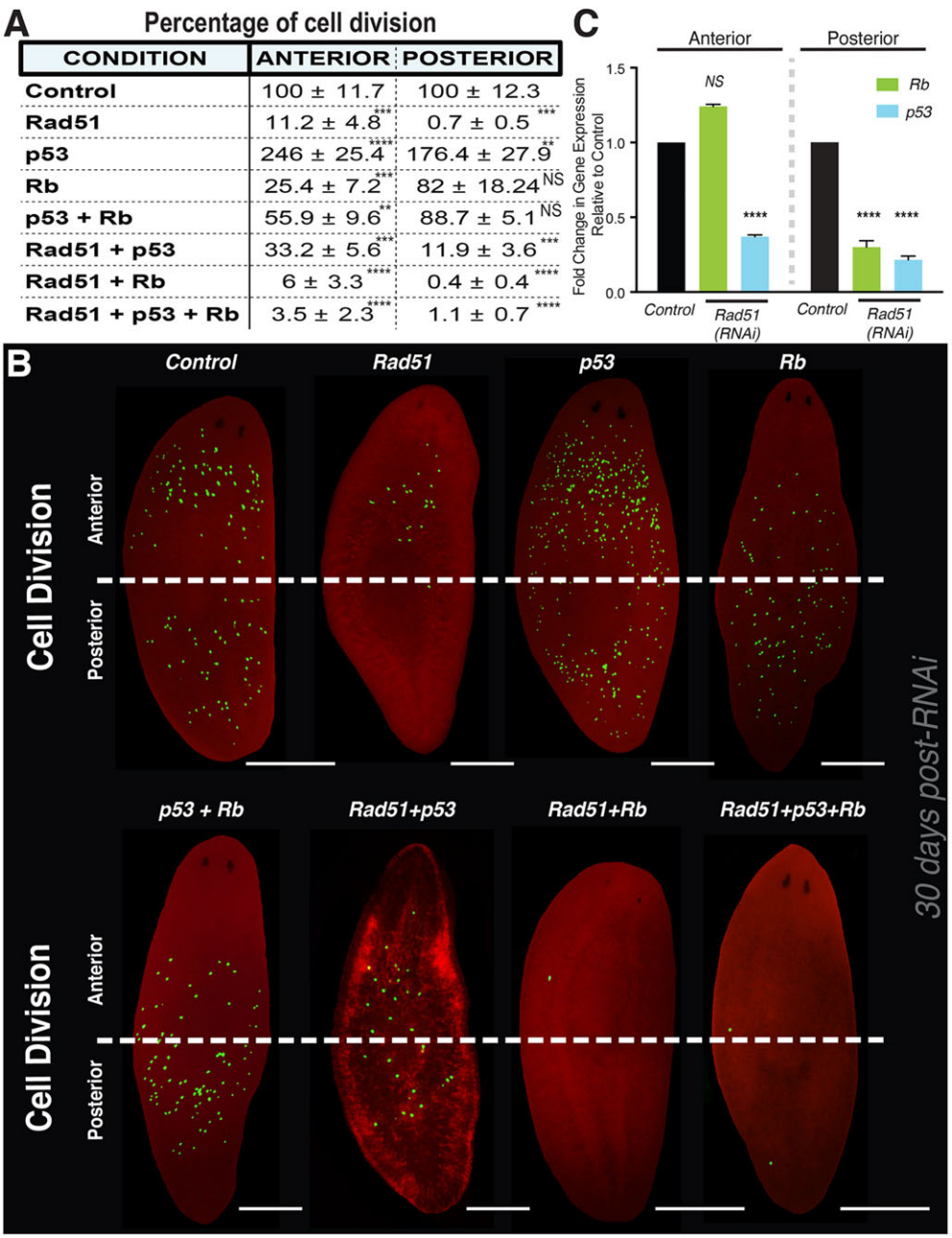

Fig. 5. The retinoblastoma (Rb) pathway mediates cell division after *Rad51(RNAi)*. (A) Percentage of cell division in anterior and posterior regions in single, double and triple RNAi treatment involving *Rad51* and the tumor suppressors *p53* and retinoblastoma (*Rb*). Simultaneous RNAi knockdown of *Rad51* and *Rb* abolish cell division in both anterior and posterior regions. (B) Representative whole-mount immunostaining images with the mitotic marker anti-H3P (green dots). Simultaneous downregulation of *p53* and *Rb* tends to concentrate cell division towards the posterior region of the animal as does *Rb(RNAi)* alone. However, *Rad51(RNAi)+Rb(RNAi)* largely reduces cell division throughout the body, even when *p53* is downregulated in triple RNAi. Each image consists of multiple focal planes stacked together to represent the entire animal (*z*-axis). Scale bars: 200 µm. (C) qPCR analysis from anterior and posterior regions to determine fold-change in *Rb* and *p53* gene expression levels in *Rad51(RNAi)* relative to control. Gene expression values were calculated relative to the ubiquitously expressed clone *H.55.12e*. In A,C, all data represent mean±s.e.m. of at least three biological replicates consisting of 10-20 animals per experiment. ****$P<0.0001$; NS, not significant; two-way ANOVA.

conserved in planarians (Pearson and Sanchez Alvarado, 2010). Increased mitotic activity in animals subjected to double p53 +Rad51 RNAi revealed cells with the potential to divide in spite of a dysfunctional homologous recombination and further established that cell division in *Rad51(RNAi)* animals occurs independently of p53. However, double Rad51+Rb RNAi knockdown abrogated cell division even when p53 was downregulated, implying that Rb is required for cell cycle progression to G2/M phase in *Rad51(RNAi)* animals (Fig. 5A,B). Interestingly, *Rad51(RNAi)* induced a strong downregulation of p53 throughout the animal accompanied by selective suppression of Rb expression in the posterior region, whereas its levels in the anterior remained stable despite high levels of DNA damage (Fig. 5C). It is possible that p53 downregulation results from the elimination of cells that are more susceptible to loss of Rad51 function, but further experiments are required to test this hypothesis. Posterior-specific levels of cell death in *Rad51(RNAi)* animals might result from the simultaneous downregulation of both p53 and Rb, which has been implicated as a driver of apoptosis in human embryonic stem cells (Conklin et al., 2012). Conversely, the presence of DNA damage and resistance to apoptosis have been suggested as an Rb-mediated mechanism of some tumor cells in response to chemotherapy (Ianari et al., 2009). Thus, it is possible that sustained levels of Rb expression in the anterior region promotes cellular survival, but more importantly, enables the proliferation of cells with damaged DNA. Future experiments assaying Rb phosphorylation as well as the activation and/or repression of components of the Rb regulatory network might lead to insights on Rb-mediated cell fate in the presence of DNA damage in adult stem cells (Sage, 2012). Taken together, our findings suggest that in the presence of genomic instability, the Rb pathway might modulate cellular fate decisions asymmetrically throughout the adult body. Similarly, these results also suggest that non-cell autonomous mechanisms operate along the anteroposterior axis to regulate Rb function.

Development (2016) 143, 1697-1709 doi:10.1242/dev.131318

Tissue-specific signals from the nervous system influence cellular behavior along the anteroposterior axis

The Rad51 phenotype is characterized by the survival of cells with DSBs in the anterior half of the animal. To address whether asymmetric cell behavior is influenced by tissue-specific signals, we produced animals with bipolar heads or tails resulting from perturbation of Wnt signaling (Reddien, 2011) (Fig. S7A-C). Furthermore, we downregulated Rad51 expression in these animals to assess levels of cell division and cell death (Fig. 6A-C). Double-headed planarians are organisms constituted by tissue from the anterior region, lacking posteriorized tissue. Double-headed animals subjected to *Rad51(RNAi)* displayed a reduction in both mitoses and cell death, and cell division was dispersed throughout the anteriorized body (Fig. 6A,B). Conversely, *Rad51(RNAi)* in double-tailed planarians (i.e. organisms lacking anterior tissue) led to a dramatic decrease of mitotic cells, accompanied by an increase in cell death (Fig. 6A,C), which was proportional to the levels of cell death found in the posterior region of *Rad51(RNAi)* animals with normal anteroposterior polarity (Fig. 3D). These results suggest tissue-specific signals in the anterior region promote cell survival in *Rad51(RNAi)* animals.

The planarian brain is located in the anterior part of the animal and occupies most of the head region (Fig. S7A). Therefore, we tested whether the presence of brain tissue might influence the proliferation of cells with DNA damage in Rad51-deficient animals. Double-tailed animals are completely posteriorized and do not possess brain-specific tissue. Thus, we ectopically induced brain formation in these organisms by disrupting the fibroblast growth factor receptor-like molecule gene *nou-darake* (*ndk*) (Iglesias et al., 2011). Double-tailed animals with ectopic brain were subjected to *Rad51(RNAi)* and evaluated for levels of cell division. We observed that the number of dividing cells increased but only in the proximity of ectopic brain tissue. Other parts of the animal that retained tail identity (i.e. devoid of brain) displayed lower levels of cellular proliferation (Fig. 6D,E; Fig. S7D,E). These results suggest: (1) the presence of anterior-specific nervous tissue in a posteriorized environment is capable of altering cell fate decisions to promote proliferation of cells with DNA damage, and (2) the central nervous system, specifically the brain, acts as a regional regulator of cell behavior in the adult planarian. The specific mechanisms need to be further investigated, but our findings suggest that non-cell autonomous signals from the cellular microenvironment might influence cell division in *Rad51(RNAi)* animals.

Cells with DNA damage overproliferate in the presence of nutrients and tissue repair demands

We sought to better understand the influence of the microenvironment on the mitotic response after *Rad51(RNAi)* treatment. Neoblasts are known to mount stereotypical waves of proliferation in response to feeding and injury (Kang and Sanchez Alvarado, 2009; Wenemoser and Reddien, 2010). Therefore, we assessed whether mitotic activity in *Rad51(RNAi)* animals could be altered by an increase in the availability of nutrients and the demands of tissue repair. Feeding triggers an increase in neoblast mitotic activity that is detected as early as 6 h post-feeding and is expected to return to pre-feeding levels by 72 h post-feeding. We found that 6 h post-feeding, cell division in *Rad51(RNAi)* animals increased ∼fivefold in both the anterior and posterior regions. However, the increase in neoblast division did not return to pre-feeding levels by 72 h post-feeding (Fig. 7A), but it was sustained and also triggered animal death >35 days post-RNAi treatment (20/20 animals, data not shown). Lethality was preceded by loss of tissue in the anterior tip of the animal, also known as 'head regression', which is characteristic of dysfunctional neoblasts and a lack of cellular turnover (Reddien et al., 2005b).

To evaluate the mitotic response upon injury, we analyzed: (1) regenerating trunk fragments after the removal of anterior and posterior tissues, and (2) tissue transplantation and the engraftment process. Amputation triggers two waves of mitotic activity (at ∼6 h and 48 h post-amputation) that are followed by cellular differentiation and formation of the regenerative blastema (Wenemoser and Reddien, 2010). Amputation of *Rad51(RNAi)* animals triggered a neoblast mitotic peak after 6 h post-amputation, which returned to pre-injury levels after 30 h. However, seven days post-amputation, levels of cell division were unexpectedly high in the absence of a regenerative blastema (Fig. 7B). The increase in cell division at seven days post-amputation and the absence of a blastema suggests that in *Rad51 (RNAi)* animals, neoblasts are unable to properly regulate cell division and their division progeny is incompetent to support post-mitotic events associated with tissue regeneration.

Tissue transplantation experiments were designed to assess the mitotic response during engraftment of tissue plugs into an orthotopic (similar) region of a host animal (Fig. 7C). This procedure allowed us to evaluate injury-induced mitotic response during tissue engraftment and regulation of cell division in the entire host animal without the formation of a regenerative blastema. We transplanted tissue plugs from both RNAi and control donors and evaluated cell division within both the host animal and within the transplanted tissue plug itself (experimental scheme is illustrated in Fig. 7C). A tissue plug from the anterior region of a donor animal was transplanted to the anterior region of a host animal. Both control and *Rad51(RNAi)* animals served as either a tissue plug donor and/or engraftment host. In all cases, levels of cell division were analyzed one week post-transplantation, at which point they would be expected to rebound to levels of uninjured animals (Fig. 7C-G).

To evaluate whether mitotic activity in the host animal returns to pre-injury levels, we first transplanted tissue plugs from the anterior donor region into the anterior region of the host (Fig. 7C). The mitotic response was quantified within the host animal excluding the transplanted tissue (i.e. outside the transplant; Fig. 7D,E). We found that tissue plugs from control donors re-established cell division in the *Rad51(RNAi)* hosts and after one week post-transplantation, levels of cell division were comparable with the control group. This suggests that transplanted cells from the donor control were able to regulate mitotic activity after engraftment in a homologous recombination-deficient host (Fig. 7E). Conversely, transplantation of *Rad51(RNAi)* donor tissue into either control or *Rad51(RNAi)* hosts elicited hyperproliferation throughout the animal (Fig. 7E; Fig. S8). These results suggest that neoblasts from *Rad51 (RNAi)* donors sense and respond to injury but are unable to regulate levels of proliferation after the completion of tissue engraftment, which is consistent with the increase of neoblast proliferation during blastema-mediated tissue regeneration (Fig. 7B).

Furthermore, we evaluated the source of abnormally proliferating cells by quantifying mitoses exclusively inside the transplanted donor plugs (i.e. excluding cellular proliferation in the rest of the host animal; Fig. 7F,G). As expected, levels of cell division in tissue plugs from control donors reverted back to the levels of uninjured animals (i.e. ∼150-200 mitoses/mm^2). However, cell division within the *Rad51(RNAi)* donor plug increased 16-fold in comparison with uninjured *Rad51(RNAi)* animals (Fig. 3B, Fig. 7G). To assess if this response is specific to homologous recombination deficiency, we also engrafted tissue plugs from NHEJ-deficient donors [*Smed-Ku70(RNAi)*] into control hosts. Mitotic activity inside the transplanted tissue plug and within the

Development (2016) 143, 1697-1709 doi:10.1242/dev.131318

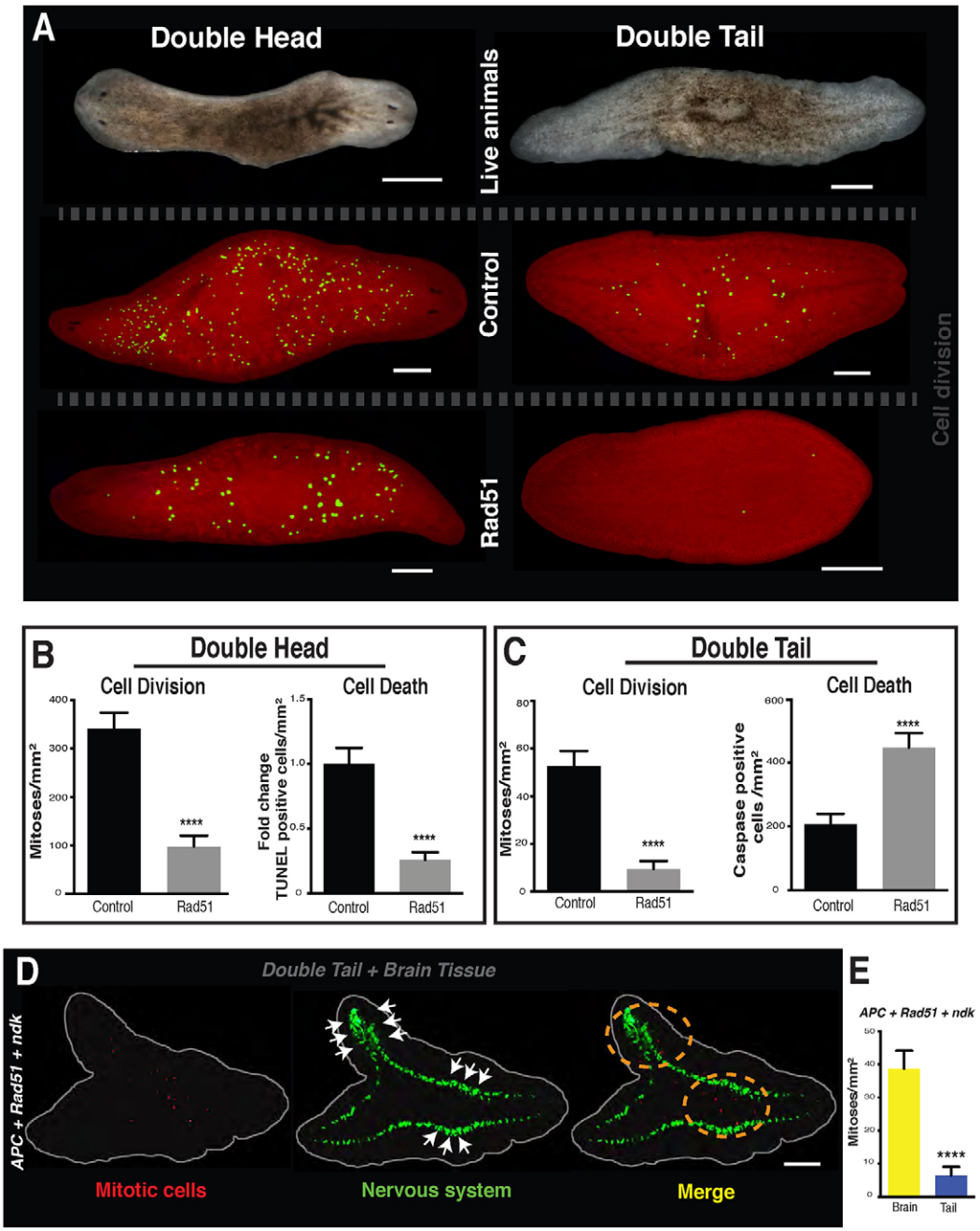

Fig. 6. Anterior-specific nervous tissue modulates cell division in posteriorized animals. (A) Downregulation of *beta-catenin* and *APC* lead to animals with bipolar heads or tails, respectively. The spatial distribution of mitotic cells (yellow dots) labelled with anti-H3P antibody is shown. (B,C) Quantification of mitoses (left) and levels of cell death (right) in double-headed (B) and double-tailed (C) animals treated with *Rad51(RNAi)*. (D,E) Cell division levels in double-tailed animals subjected to double RNAi with *nou-darake* and *Rad51* knockdown. Brain tissue (arrows) and ventral nerve cords were labeled with anti-synapsin staining (green signal). The dotted orange line illustrates an area contiguous to the ectopic brain, including mitotic cells (red dots). Brain tissue was identified by visual thickening of the ventral nerve cords. Scale bars: 200 µm. In B,C,E, data represent mean±s.e.m. of at least three biological replicates with n>5-10 animals per experiment. ****P<0.0001 one-way ANOVA.

host was similar to that of the control group after one week post-transplantation (data not shown). These results imply that neoblast hyperproliferation upon injury and/or engraftment is not a result of off-target RNAi effects, but is a specific feature of homologous recombination-deficient cells. Taken together, our findings confirm that in the presence of injury, neoblasts from *Rad51(RNAi)* animals intensify their proliferation capabilities, probably through cell-autonomous mechanisms, but are unable to return to uninjured levels once tissue repair is completed. We also demonstrate that despite high levels of DNA damage, neoblasts sense environmental cues triggered by metabolic and tissue repair signals that override cellular fate decisions imposed by DNA damage (Fig. 7A,B).

We hypothesize that the hyperproliferative state of these cells could be triggered by a defective response that circumvents a block in cell cycle progression in favor of tissue renewal and repair (Bartkova et al., 2006). Moreover, gene expression analysis revealed that markers of the zeta class of neoblasts (van Wolfswinkel et al., 2014) were the least downregulated in the anterior part of *Rad51(RNAi)* animals,

Development (2016) 143, 1697-1709 doi:10.1242/dev.131318

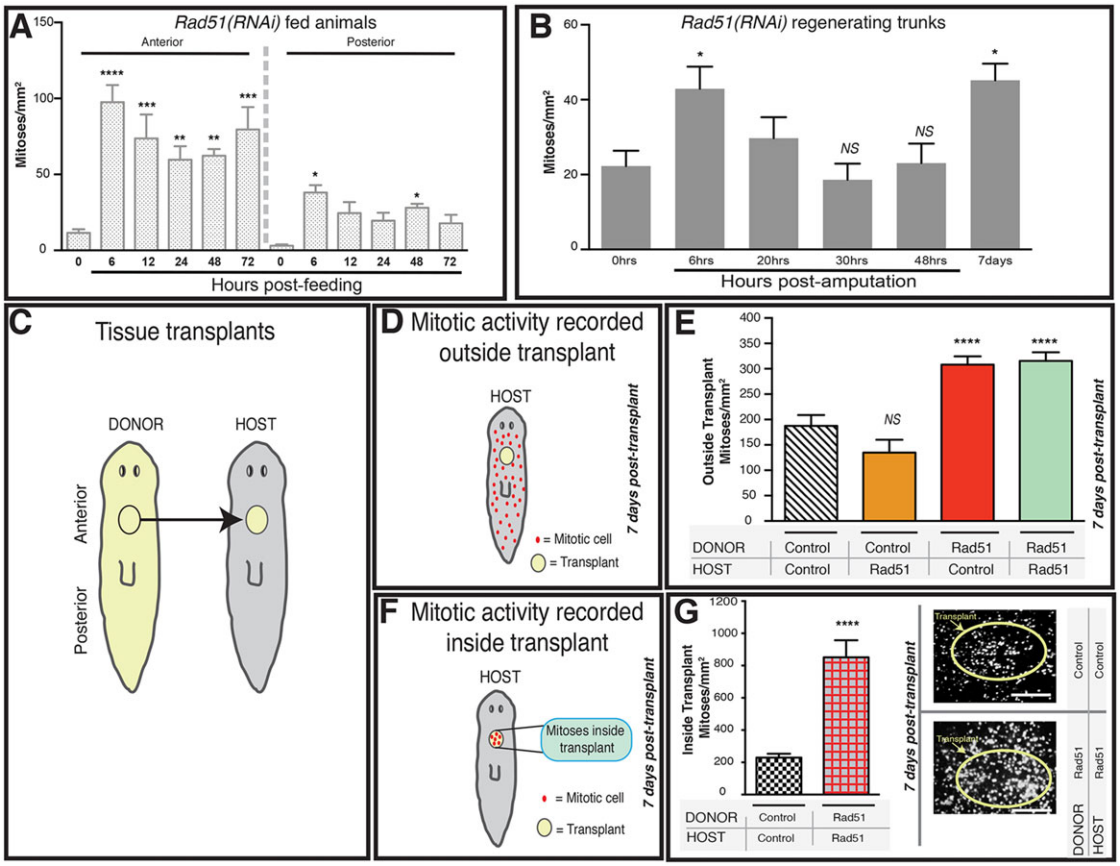

Fig. 7. Metabolic signals and demands for tissue repair trigger neoblast hyperproliferation. (A,B) Mitotic activity increases 6 h after feeding (A) or amputation (B) in *Rad51(RNAi)* animals. Mitotic cells were recorded in both anterior and posterior regions after feeding, whereas in amputated animals the overall number of cells was obtained from regenerating trunk fragments. (C) Schematic representation of tissue plug transplants from the anterior region of donor animals into host animals (arrow). (D) Schematic representation to evaluate mitotic activity (red dots) in the host animal excluding the transplanted tissue plug (yellow circle). (E) Levels of mitotic activity outside of the transplanted plug. Control and *Rad51(RNAi)* animals serve as either tissue plug donor and/or engraftment host. Notice the increased cell division when donor tissue comes from *Rad51(RNAi)* animals. (F) Donor tissue from the anterior region was transplanted into an orthotopic region in host animals and was used to determine levels of cell division inside the transplant. (G) Quantification of mitotic activity inside the transplanted plug, one week after engraftment (left panel). Representative pictures showing mitotic activity inside the transplant (right panel; yellow circles represent the transplant border). Mitotic activity was recorded 7 days after transplantation, when they are expected to be back to levels of uninjured animals. Scale bar: 250 µm. In A,B,E,G, data represent mean±s.e.m. of at least three biological replicates with n>5-10 animals per time point. *P<0.01, **P<0.005, ***P<0.0005. ****P<0.0001; NS, not significant; Tukey's multiple comparison test.

suggesting the phenotype is not homogeneously distributed among neoblast subpopulations (Fig. S9). However, additional experiments are required to rule out whether the hyperproliferative state in *Rad51 (RNAi)* animals is related to a particular neoblast subpopulation. Additional experiments on the Rad51 phenotype in *S. mediterranea* would facilitate the identification and characterization of molecular mechanisms mediating cell division in the presence of DNA damage (Campisi, 2005).

Concluding remarks

The DNA damage response is a potent regulator of cellular behavior that influences decisions about proliferation and apoptosis (Halazonetis et al., 2008; Lord and Ashworth, 2012). The Rad51 phenotype establishes a predictable model where cells with genomic instability undergo collective elimination by apoptosis, alter cell cycle patterns, or bypass surveillance mechanisms to divide and even hyperproliferate. Our results indicate that both cellular location along the anteroposterior axis (non-autonomous) and intrinsic cellular (cell-autonomous) properties modulate cellular fate choices in the presence of DNA damage.

Injury-induced cell proliferation is still activated after downregulation of Rad51, but subsequent mechanisms regulating proliferation fail to return or maintain basal mitotic levels (i.e. cell division to support homeostatic tissue renewal). Consequently, cells with damaged DNA divide abnormally following both cell autonomous and non-autonomous cues. Our results present novel insights into the effects of system-wide Rad51 downregulation in adult tissue maintenance. Thus, we anticipate that further research in the Rad51 phenotype in *S. mediterranea* would facilitate opportunities to analyze *in situ* DNA damage-induced tumor suppression, mechanisms regulating proliferation of cells with genomic instability, and the provocative idea of nervous signals controlling tumor suppressor regulatory networks in specific regions of the adult body.

MATERIALS AND METHODS

Identification of homologs and phylogenetic analysis

Components of the DNA repair and other signaling pathways were identified using the *S. mediterranea* genome database SmedGD (http://smedgd.stowers.org) and other planarian genomic resources (Adamidi et al.,

Development (2016) 143, 1697-1709 doi:10.1242/dev.131318

2011; Labbe et al., 2012; Robb et al., 2008; Sandmann et al., 2011; Zhu and Pearson, 2013). NCBI accession numbers KT375434 (*Smed-ku70*), KT375435 (*Smed-BRCA2*), KT375436 (*Smed-Mre11*) and SmedGD references mk4.001927.02.01, mk4.001165.06.01 (SmedGD v.3.1) are linked to sequences reported in the manuscript. Identified sequences were translated using the Pfam protein domain families database (http://pfam.xfam.org/) and subsequently analyzed using HMMER search to confirm conservation (https://www.ebi.ac.uk/Tools/hmmer/). The sequences were further confirmed by Blastn, blastx, blastp and alignment tools (http://blast.ncbi.nlm.nih.gov/Blast.cgi). The identified sequences were aligned by CLUSTALW or T-Coffee software with sequences obtained using HomoloGene (http://www.ncbi.nlm.nih.gov/homologene). A predictive evolutionary model and phylogenetic tree was built using MEGA software (www.megasoftware.net).

Planarian culture

The planarian species used in these experiments was *Schmidtea mediterranea* CIW4. *S. mediterranea* culture was maintained as previously described (Oviedo et al., 2008a).

RNAi experiments

The synthesis of dsRNA was performed *in vitro* followed by microinjections as previously described (Oviedo and Levin, 2007; Oviedo et al., 2008b). A total of five microinjections over four weeks were initially administered over three consecutive days and then one every 10 days. Alternatively, *in vitro* synthesized dsRNA was also administered by feeding to functionally disrupt genes by RNAi as described (Rouhana et al., 2013). Briefly, 1 µg of the *Smed-Rad51*-specific dsRNA was mixed with 30 µl of planaria food and was fed 3× times per week for 30 days. Although RNAi by feeding or microinjection in different areas of the body both efficiently reduced Rad51 expression, the experiments presented throughout the manuscript involved dsRNA microinjections in the anterior area unless otherwise noted. Under this protocol 100% of the animals showed the phenotype between 20-30 days after first dsRNA microinjection. All analyses were carried out a minimum of four days after the last microinjection. To produce animals with double head or tails, planaria were fed bacteria with engineered vectors as previously described (Reddien et al., 2005a). Briefly, downregulation of APC and β-catenin by RNAi was performed using 4-6 feedings before amputation. After 14 days of regeneration bipolar headed/tailed animals were injected with the desired dsRNA as described in Fig. S10. Dr C. Petersen (Northwestern University, Evanston, IL, USA) and Dr P. Reddien (MIT, Cambridge, MA, USA) kindly provided β-catenin and APC plasmids. Double and triple RNAi experiments were analyzed 30 days after the first *Rad51* dsRNA microinjection as shown in Fig. S10.

Whole-mount immunofluorescence

Planarians were fixed and immunostained as previously described (Peiris et al., 2012). The following primary antibodies were used: anti-H3p (1:250; Millipore, 05-817R), anti-synapsin (1:100; Developmental Studies Hybridoma Bank) and anti-activated caspase-3 (1:500; Abcam, ab13847). Secondary antibodies were: goat anti-mouse Alexa Fluor 488 (1:800; Invitrogen, 673781) for anti-synapsin, anti-arrestin, anti-acetylated tubulin, goat anti-rabbit Alexa Fluor 568 (1:800; Invitrogen, 11036) for anti-H3P, HRP-conjugated goat anti-rabbit antibody (1:2000; Millipore, 12-348) with TSA-Alexa Fluor 488 anti-HRP (ThermoFisher, A-21370) for anti-caspase-3. All images were visualized and the mitotic cells (H3P-positive) and apoptotic cells (caspase-positive) were counted and normalized to the area (mm^2) using NIS element software (Nikon).

BrdU staining

BrdU staining was performed as previously described (Cowles et al., 2012). Double staining with H3P and BrdU was performed as previously described (Newmark and Sanchez Alvarado, 2000).

Sub-cloning of candidate genes

Our sub-cloning strategy was similar to that previously described (Peiris et al., 2012). Briefly, sets of primers were designed to amplify a 400-650 bp region of each candidate gene. Total RNA from asexual *S. mediterranea* was used to synthesize cDNA using Thermo Scientific Verso cDNA kit. The amplified regions were cloned and transformed following the manufacturer's instructions (Qiagen). PCR products were used to synthesize dsRNA or ISH probes as previously described (Oviedo et al., 2008b; Peiris et al., 2012). Primers sequences are listed in Table S1.

Planaria dissociation and cell collection

Planarians were dissociated as previously described with slight modifications (Hayashi et al., 2006; Peiris et al., 2016; Reddien et al., 2005b). Planarians were amputated into small pieces in cold calcium/magnesium-free (CMF) medium and then placed on a rocker for 30 min to 1 h at 4°C. Cells were filtered using a 20 µm filter and centrifuged at 239 ***g*** followed by resuspension in 1 ml of CMF media before cell counting (Peiris et al., 2016).

Fixation and immunostaining of dissociated cells

Fixation and staining protocol were as previously described (Oviedo and Levin, 2007; Peiris et al., 2012). Dissociated cells were washed twice with 1× PBS and then fixed onto cover slips using Carnoy's fixation for 2 h on ice, incubated with 100% methanol for 1 h at −20°C. Samples were rehydrated using mixtures of 75%, 50% and 25% methanol in PBSTx (1×PBS+0.3% Triton X-100). After final rehydration with 100% PBSTx, the cells were blocked in PBSTB [1×PBS+0.3% Triton X-100 containing 0.25% bovine albumin serum (BSA)] for 4 h at room temperature and primary anti-Rad51 (1:500; Abcam, ab109107) antibody added overnight. Cells were then washed six times, 10 min each in PBSTB and then stained with HRP-conjugated goat anti-rabbit secondary antibody (1:500; Millipore, 12-348) overnight. Cells were then washed again, and incubated with 1:1000 TSA-Alexa Fluor 488 in PBSTI (PBST×+10 mM imidazole) for 20 min, followed by a further six 10 min washes in PBSTB. After the final wash, cells were incubated with DAPI (0.1 µg/1 ml) for 15 min and mounted using VECTASHIELD Mounting Medium (Vector Laboratories). Additional details can be found in our previous publication (Oviedo and Levin, 2007; Peiris et al., 2012).

Protein extraction

Animals were dissociated until no tissue fragments were visible and incubated in 1× RIPA buffer (Cell Signaling Technologies, 9806) with protease inhibitors (Roche Complete Mini Protease Inhibitor Cocktail, 04693124001; 1 mM PMSF; 1 mM DTT) for 30 min on ice. Volume-to-mass ratio for this was as follows: 10 large dissociated planaria were incubated in 300 µl of 1× RIPA and protease cocktail mixture. Samples were spun at 20,817 ***g*** for 15 min at 4°C. The supernatant was transferred to a new tube and immediately placed on ice. A 25 µl aliquot of the supernatant was used to measure protein concentration. The remaining solution was mixed with equal volumes of 2× Laemmli buffer (4% SDS, 10% 2-mercaptoethanol, 20% glycerol, 0.004% bromophenol blue, 0.125 M Tris-HCl) and incubated at 95°C for 5 min (or boiled at 100°C) to denature and reduce. Protein lysates were stored at −20°C. A Bio-Rad protein assay was used to determine protein concentration.

Western blot

Protein lysate aliquots of 40 µg were heated at 80°C for 5 min and loaded in 12.5-15% SDS-PAGE gel along with a molecular weight marker (Bio-Rad, 1610375). Samples were transferred to a 30 s methanol-activated PVDF membrane (Bio-Rad, 162-0175) overnight in 1× Tris-glycine transfer buffer [25 mM Tris base, 192 mM glycine, 10% (v/v) methanol, pH 8.3] at 4°C. The membrane was blocked with 5% milk for 1 h and incubated in the primary antibodies overnight at 4°C on a rocker. Primary antibodies: anti-tubulin (1:500; Sigma, 081M4861), anti-Rad51 (1:5000; Abcam, ab109107) and anti-caspase (1:5000; Abcam, ab13847). The membrane was washed three times for 30 min prior to the addition of the secondary antibodies: HRP-conjugated goat anti-rabbit antibody (1:2000; Millipore, 12-348) for anti-Rad51 and anti-caspase, HRP-conjugated goat anti-mouse antibody (1:2000; Invitrogen, G21040) for anti-tubulin. The membrane was washed three times for 30 min and developed using Luminata Forte Western HRP substrate (Millipore, WBLUF0100).

Development (2016) 143, 1697-1709 doi:10.1242/dev.131318

Flow cytometry analysis

Flow cytometry experiments were performed as previously described (Hayashi et al., 2006; Peiris et al., 2016, 2012). Briefly, 1×10^6 cells from dissociated planaria were stained with DNA marker Draq5 (eBioscience, 65-0880-96) at a 1:500 dilution in CMF media for 30 min at room temperature in the dark. Incubation with calcein (Invitrogen, C3100MP) diluted 1:500 in CMF medium for 10 min at room temperature was sufficient to stain live cells. BD FACSDiva software was used for initial gating and samples were either analyzed using a LSRII flow cytometer (BD Biosciences) or sorted using an ARIAII flow cytometer (BD Biosciences). Lethally irradiated planaria were used to approximate the gates for X1 and X2 populations and/or gated as previously described (Eissenhoffer et al., 2008). Final gating of cell populations was performed using FlowJo software (www.flowjo.com) (Peiris et al., 2016).

Cell cycle analysis was performed using either Draq5 (1:500 diluted in CMF media) or DAPI (0.1 µg/ml). Draq5-stained populations were gated for cell cycle using live Draq5-positive populations and FlowJo software. Staining of apoptotic cells was performed using 1×10^5 cells from dissociated planaria immersed in 100 µl binding buffer (BioLegend, 422201) and stained with 5 µl Annexin V (Pacific Blue; BioLegend, 640918) and 5 µl 7-AAD Viability Staining Solution (PECy5; BioLegend, 420404). Labeled cells were incubated at room temperature for 15 min. The samples were immediately analyzed using an LSRII flow cytometer (BD Biosciences). Further details can be found in Peiris et al. (2016).

TUNEL assay

TUNEL assay was performed as previously described (Pellettieri et al., 2010).

Quantification of mitotic activity and image processing

Mitotic cells labeled with fluorescent anti-H3P were counted either manually or with NIS Elements (Nikon). Area measurements for the anterior and posterior regions in each sample were obtained with NIS Elements (Nikon). All fluorescence images consisted of multiple captions at different focal planes (*z*-axis) and stacked together into a single image to represent the whole animal. Cellular counts or fluorescence signal from images at different magnifications were corrected by area to determine the specific number/mm^2. The analysis of anterior and posterior regions was paired to its respective counterpart (i.e. control anterior versus experimental anterior; control posterior versus experimental posterior) and pooled numbers were plotted separately. Additional details on the procedure and image processing were as previously described (Peiris et al., 2012).

Quantitative RT-PCR

Quantitative RT-PCR (qPCR) was performed as previously described (Peiris et al., 2012). In all cases gene expression is relative to the ubiquitously expressed clone *H.55.12e*. Each individual experiment consisted of triplicates per condition and experiments were independently repeated at least twice. qPCR from sorted cells was obtained by dissociating >20 animals per condition to extract RNA and prepare cDNA as described before. qPCR from anterior and posterior regions was prepared from half body parts of more than 10 animals per condition. Gene expression up- or downregulation levels were also represented with heat maps in reference to the corresponding control. Gene expression corresponds to the mean of triplicated samples of at least two independent experiments with pooled RNA extraction of >20 animals each.

In situ hybridization (ISH)

ISH on isolated cells and quantification were performed as previously described (Oviedo and Levin, 2007; Oviedo et al., 2008c). Whole-mount ISH (WISH) and fluorescent *in situ* hybridization were performed as previously described (Pearson et al., 2009).

Comet assay

Dr Dave Alexander and Dr Manel Camps from University of California Santa Cruz kindly provided the comet assay protocol and Elyse Ozamoto (University of California, Merced, USA) performed the initial adaptations to the planarian model. Frosted microscope slides were coated with 1% normal melting point agarose (NMPA) in 10× PBS and dried overnight. Dissociated cells were resuspended in 10 ml CMF followed by incubation at 37°C for 2 hours. Cells were centrifuged at 664 ***g*** for 2 min and resuspended in 100 µl of 0.5% low melting point agarose (LMPA) made in 10× PBS per 50,000 cells. The mixture was loaded onto coated 1% NMPA dried slides and allowed to dry at 4°C until the agarose solidified. Slides were incubated overnight in a Coplin jar at 4°C with 89% lysing solution (2.5 M NaCl, 100 mM EDTA, 10 mM Trizma base, 8 g pelletized NaOH in dH_2O; filtered and pH 10.0), 10% DMSO and 1% Triton X-100. Medium was then replaced with neutralization buffer (0.4 M Tris base in dH_2O, pH to 7.5) for 5 min and kept at 4°C. The neutralization buffer was then removed and slides were placed into an electrophoresis chamber at 4°C filled with 1× electrophoresis buffer (10 N NaOH and 200 mM EDTA in dH_2O, pH 13) and the sample was allowed to equilibrate for 15 min. The current was adjusted to 12 V for 30 min at 4°C. Next, slides were transferred back into the Coplin jar and equilibrated for 5 min in neutralization buffer. Samples were fixed with cold 100% ethanol for 5 min and stained with a 1:10 ratio of SYBR gold into 1× TE buffer (10 mM Tris-HCl and 1 mM EDTA, pH 7.5). A standard 'DNA damage scale' was built as reference based on different doses of gamma irradiation on whole worms. The scoring scheme is based on a rank from 0 to 2, where a score of 0 showed little DNA damage and 2 is visualized as a disbursed tail, indicating extensive DNA damage (Sinha et al., 2014).

Karyotyping assay and tissue transplantation experiments

Karyotyping and tissue transplants were performed as previously described (Guedelhoefer and Sanchez Alvarado, 2012). The worms for transplantation experiments were grown at 10°C to obtain larger animals more amenable for transplantation. Similar sizes of the transplanted tissue and the opening in the host animals were obtained by using the tip of 10 µl pipettes. Animals that served as donors or hosts were used after 30 days of the first dsRNA microinjection.

Statistical analysis

Data are expressed as mean±s.e.m. unless otherwise noted. The statistical analyses were performed in Prism, GraphPad Software (http://www.graphpad.com).

Acknowledgements

We thank Edelweiss Pfister for technical assistance, members of the planarian community for reagents, and Drs Manel Camps and David Alexander for advice with comet assay. N.J.O. also thanks Drs Julien Sage, Aaron Hernday, Ramen Saha, Kirk Jensen, Jennifer Manilay, Michael Cleary, Michael Urner, and members of the Oviedo Lab for comments on the manuscript.

Competing interests

The authors declare no competing or financial interests.

Author contributions

T.H.P., D.R., P.G.B., U.O., D.D., F.W. and N.J.O. performed the research and analyzed data. N.J.O. conceived the project and wrote the manuscript with P.G.B. All authors read the manuscript and provided comments.

Funding

We acknowledge support from University of California Merced, University of California Cancer Research Coordinating Committee, Health Sciences Research Institute at University of California, Merced and awards from Jane Vilas and the Hellman Fellows Fund. This research was supported by the National Cancer Institute and National Institute of General Medical Sciences of the National Institutes of Health [CA176114 and GM109372 to N.J.O.]. Deposited in PMC for release after 12 months.

Supplementary information

Supplementary information available online at
http://dev.biologists.org/lookup/suppl/doi:10.1242/dev.131318/-/DC1

References

Adamidi, C., Wang, Y., Gruen, D., Mastrobuoni, G., You, X., Tolle, D., Dodt, M., Mackowiak, S. D., Gogol-Doering, A., Oenal, P. et al. (2011). De novo assembly and validation of planaria transcriptome by massive parallel sequencing and shotgun proteomics. *Genome Res.* **21**, 1193-1200.

Auerbach, R. and Auerbach, W. (1982). Regional differences in the growth of normal and neoplastic cells. *Science* **215**, 127-134.
Auerbach, R., Morrissey, L. W. and Sidky, Y. A. (1978). Regional differences in the incidence and growth of mouse tumors following intradermal or subcutaneous inoculation. *Cancer Res.* **38**, 1739-1744.
Baguñà, J. (1976). Mitosis in the intact and regenerating planarian *Dugesia mediterranea* n.sp. I. Mitotic studies during growth, feeding and starvation. *J. Exp. Zool.* **195**, 53-64.
Bartkova, J., Rezaei, N., Liontos, M., Karakaidos, P., Kletsas, D., Issaeva, N., Vassiliou, L.-V., Kolettas, E., Niforou, K., Zoumpourlis, V. C. et al. (2006). Oncogene-induced senescence is part of the tumorigenesis barrier imposed by DNA damage checkpoints. *Nature* **444**, 633-637.
Brøndsted, H. V. (1969). *Planarian Regeneration*, 1st edn. London: Pergamon Press.
Campisi, J. (2005). Senescent cells, tumor suppression, and organismal aging: good citizens, bad neighbors. *Cell* **120**, 513-522.
Chinone, A. and Matsumoto, M. (2014). DrRad51 is required for chiasmata formation in meiosis in planarian Dugesia ryukyuensis. *Mol. Reprod. Dev.* **81**, 409-421.
Conklin, J. F., Baker, J. and Sage, J. (2012). The RB family is required for the self-renewal and survival of human embryonic stem cells. *Nat. Commun.* **3**, 1244.
Cowles, M. W., Hubert, A. and Zayas, R. M. (2012). A Lissencephaly-1 homologue is essential for mitotic progression in the planarian *Schmidtea mediterranea*. *Dev. Dyn.* **241**, 901-910.
Dispersio, L. P. (1981). Regional growth differences of human tumor xenografts in nude mice. *Lab. Anim.* **15**, 179-180.
Eisenhoffer, G. T., Kang, H. Sánchez Alvarado, A., (2008). Molecular analysis of stem cells and their descendants during cell turnover and regeneration in the planarian Schmidtea mediterranea. *Cell Stem Cell* **11**, 327-339.
Guedelhoefer, O. C., IV and Sanchez Alvarado, A. (2012). Amputation induces stem cell mobilization to sites of injury during planarian regeneration. *Development* **139**, 3510-3520.
Halazonetis, T. D., Gorgoulis, V. G. and Bartek, J. (2008). An oncogene-induced DNA damage model for cancer development. *Science* **319**, 1352-1355.
Hayashi, T., Asami, M., Higuchi, S., Shibata, N. and Agata, K. (2006). Isolation of planarian X-ray-sensitive stem cells by fluorescence-activated cell sorting. *Dev. Growth Differ.* **48**, 371-380.
Ianari, A., Natale, T., Calo, E., Ferretti, E., Alesse, E., Screpanti, I., Haigis, K., Gulino, A. and Lees, J. A. (2009). Proapoptotic function of the retinoblastoma tumor suppressor protein. *Cancer Cell* **15**, 184-194.
Iglesias, M., Almuedo-Castillo, M., Aboobaker, A. A. and Saló, E. (2011). Early planarian brain regeneration is independent of blastema polarity mediated by the Wnt/beta-catenin pathway. *Dev. Biol.* **358**, 68-78.
Kang, H. and Sanchez Alvarado, A. (2009). Flow cytometry methods for the study of cell-cycle parameters of planarian stem cells. *Dev. Dyn.* **238**, 1111-1117.
Klein, H. L. (2008). The consequences of Rad51 overexpression for normal and tumor cells. *DNA Repair* **7**, 686-693.
Kobayashi, K. (1977). Effects of whole-body and partial-body X irradiation upon epidermal mitotic activity during wound healing in mouse skin. *Radiat. Res.* **69**, 513-529.
Kubai, L. and Auerbach, R. (1980). Regional differences in the growth of skin transplants. *Transplantation* **30**, 128-131.
Labbe, R. M., Irimia, M., Currie, K. W., Lin, A., Zhu, S. J., Brown, D. D. R., Ross, E. J., Voisin, V., Bader, G. D., Blencowe, B. J. et al. (2012). A comparative transcriptomic analysis reveals conserved features of stem cell pluripotency in planarians and mammals. *Stem Cells* **30**, 1734-1745.
Lachiewicz, A. M., Berwick, M., Wiggins, C. L. and Thomas, N. E. (2008). Survival differences between patients with scalp or neck melanoma and those with melanoma of other sites in the Surveillance, Epidemiology, and End Results (SEER) program. *Arch. Dermatol.* **144**, 515-521.
Lim, D. S. and Hasty, P. (1996). A mutation in mouse rad51 results in an early embryonic lethal that is suppressed by a mutation in p53. *Mol. Cell. Biol.* **16**, 7133-7143.
Lord, C. J. and Ashworth, A. (2012). The DNA damage response and cancer therapy. *Nature* **481**, 287-294.
Macheret, M. and Halazonetis, T. D. (2015). DNA replication stress as a hallmark of cancer. *Annu. Rev. Pathol.* **10**, 425-448.
Newmark, P. A. and Sanchez Alvarado, A. (2000). Bromodeoxyuridine specifically labels the regenerative stem cells of planarians. *Dev. Biol.* **220**, 142-153.
Onal, P., Grun, D., Adamidi, C., Rybak, A., Solana, J., Mastrobuoni, G., Wang, Y., Rahn, H.-P., Chen, W., Kempa, S. et al. (2012). Gene expression of pluripotency determinants is conserved between mammalian and planarian stem cells. *EMBO J.* **31**, 2755-2769.
Oviedo, N. J. and Levin, M. (2007). smedinx-11 is a planarian stem cell gap junction gene required for regeneration and homeostasis. *Development* **134**, 3121-3131.
Oviedo, N. J., Nicolas, C. L., Adams, D. S. and Levin, M. (2008a). Establishing and maintaining a colony of planarians. *CSH Protoc.* **2008**, pdb prot5053.
Oviedo, N. J., Nicolas, C. L., Adams, D. S. and Levin, M. (2008b). Gene knockdown in planarians using RNA interference. *CSH Protoc.* **2008**, pdb prot5054.
Oviedo, N. J., Pearson, B. J., Levin, M. and Sánchez Alvarado, A. (2008c). Planarian PTEN homologs regulate stem cells and regeneration through TOR signaling. *Dis. Model. Mech.* **1**, 131-143.
Oviedo, N. J., Morokuma, J., Walentek, P., Kema, I. P., Gu, M. B., Ahn, J.-M., Hwang, J. S., Gojobori, T. and Levin, M. (2010). Long-range neural and gap junction protein-mediated cues control polarity during planarian regeneration. *Dev. Biol.* **339**, 188-199.
Pearson, B. J. and Sanchez Alvarado, A. (2010). A planarian p53 homolog regulates proliferation and self-renewal in adult stem cell lineages. *Development* **137**, 213-221.
Pearson, B. J., Eisenhoffer, G. T., Gurley, K. A., Rink, J. C., Miller, D. E. and Sanchez Alvarado, A. (2009). Formaldehyde-based whole-mount in situ hybridization method for planarians. *Dev. Dyn.* **238**, 443-450.
Peiris, T. H., Weckerle, F., Ozamoto, E., Ramirez, D., Davidian, D., Garcia-Ojeda, M. E. and Oviedo, N. J. (2012). TOR signaling regulates planarian stem cells and controls localized and organismal growth. *J. Cell Sci.* **125**, 1657-1665.
Peiris, T. H., Garcia-Ojeda, M. E. and Oviedo, N. J. (2016). Alternative flow cytometry strategies to analyze stem cells and cell death in planarians. *Regeneration* [Epub ahead of print] .
Pellettieri, J., Fitzgerald, P., Watanabe, S., Mancuso, J., Green, D. R. and Sanchez Alvarado, A. (2010). Cell death and tissue remodeling in planarian regeneration. *Dev. Biol.* **338**, 76-85.
Reddien, P. W. (2011). Constitutive gene expression and the specification of tissue identity in adult planarian biology. *Trends Genet.* **27**, 277-285.
Reddien, P. W., Bermange, A. L., Murfitt, K. J., Jennings, J. R. and Sanchez Alvarado, A. (2005a). Identification of genes needed for regeneration, stem cell function, and tissue homeostasis by systematic gene perturbation in planaria. *Dev. Cell* **8**, 635-649.
Reddien, P. W., Oviedo, N. J., Jennings, J. R., Jenkin, J. C. and Sanchez Alvarado, A. (2005b). SMEDWI-2 is a PIWI-like protein that regulates planarian stem cells. *Science* **310**, 1327-1330.
Robb, S. M. C., Ross, E. and Sanchez Alvarado, A. (2008). SmedGD: the *Schmidtea mediterranea* genome database. *Nucleic Acids Res.* **36**, D599-D606.
Rouhana, L., Weiss, J. A., Forsthoefel, D. J., Lee, H., King, R. S., Inoue, T., Shibata, N., Agata, K. and Newmark, P. A. (2013). RNA interference by feeding in vitro-synthesized double-stranded RNA to planarians: methodology and dynamics. *Dev. Dyn.* **242**, 718-730.
Sage, J. (2012). The retinoblastoma tumor suppressor and stem cell biology. *Genes Dev.* **26**, 1409-1420.
Sandmann, T., Vogg, M. C., Owlarn, S., Boutros, M. and Bartscherer, K. (2011). The head-regeneration transcriptome of the planarian *Schmidtea mediterranea*. *Genome Biol.* **12**, R76.
Sinha, M., Jang, Y. C., Oh, J., Khong, D., Wu, E. Y., Manohar, R., Miller, C., Regalado, S. G., Loffredo, F. S., Pancoast, J. R. et al. (2014). Restoring systemic GDF11 levels reverses age-related dysfunction in mouse skeletal muscle. *Science* **344**, 649-652.
Solana, J., Kao, D., Mihaylova, Y., Jaber-Hijazi, F., Malla, S., Wilson, R. and Aboobaker, A. (2012). Defining the molecular profile of planarian pluripotent stem cells using a combinatorial RNAseq, RNA interference and irradiation approach. *Genome Biol.* **13**, R19.
Tseng, W. H. and Martinez, S. R. (2011). Tumor location predicts survival in cutaneous head and neck melanoma. *J. Surg. Res.* **167**, 192-198.
Tsuzuki, T., Fujii, Y., Sakumi, K., Tominaga, Y., Nakao, K., Sekiguchi, M., Matsushiro, A., Yoshimura, Y. and Morita, T. Y. (1996). Targeted disruption of the Rad51 gene leads to lethality in embryonic mice. *Proc. Natl. Acad. Sci. USA* **93**, 6236-6240.
van Wolfswinkel, J. C., Wagner, D. E. and Reddien, P. W. (2014). Single-cell analysis reveals functionally distinct classes within the planarian stem cell compartment. *Cell Stem Cell* **15**, 326-339.
Wagner, D. E., Wang, I. E. and Reddien, P. W. (2011). Clonogenic neoblasts are pluripotent adult stem cells that underlie planarian regeneration. *Science* **332**, 811-816.
Wenemoser, D. and Reddien, P. W. (2010). Planarian regeneration involves distinct stem cell responses to wounds and tissue absence. *Dev. Biol.* **344**, 979-991.
Xiang, Y., Miller, D. E., Ross, E. J., Sanchez Alvarado, A. and Hawley, R. S. (2014). Synaptonemal complex extension from clustered telomeres mediates full-length chromosome pairing in *Schmidtea mediterranea*. *Proc. Natl. Acad. Sci. USA* **111**, E5159-E5168.
Zhu, S. J. and Pearson, B. J. (2013). The Retinoblastoma pathway regulates stem cell proliferation in freshwater planarians. *Dev. Biol.* **373**, 442-452.

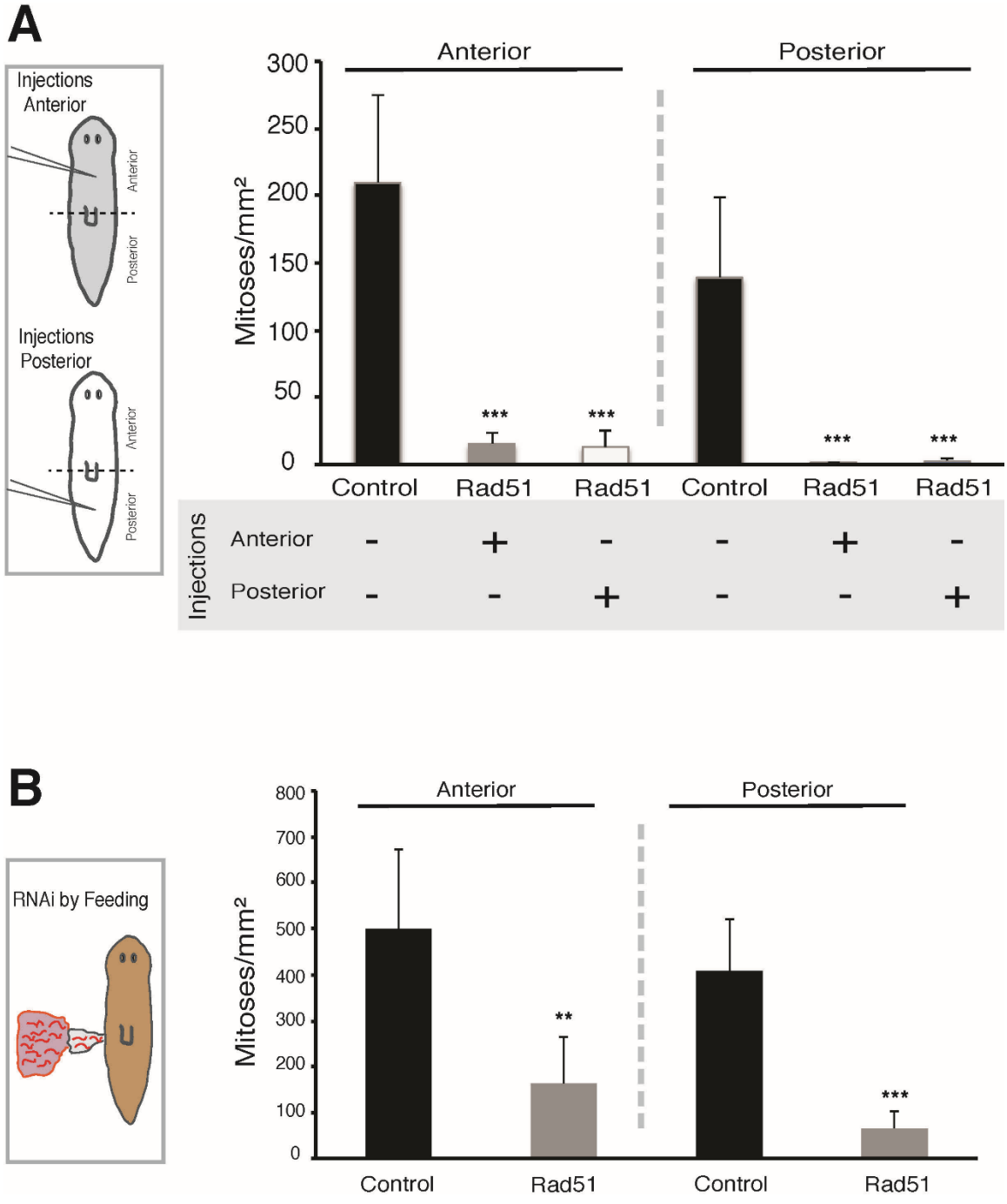

Fig. S1. Different methods of *Rad51(RNAi)* restrict cell division along the AP axis. (A) Depicts the effects of microinjections of Rad51 dsRNA in either anterior or posterior regions (represented by cartoons on the left gray and white, respectively) over mitotic activity along the AP axis. **(B)** Feeding Rad51 dsRNA synthesized *in vitro* reduces mitotic activity asymmetrically in the planarian body. Values represent mean±s.e.m. of at least two independent experiments, *n>10* animals per experiment. ****P<0.0001*, ***P<0.001* by Tukey's multiple comparison test.

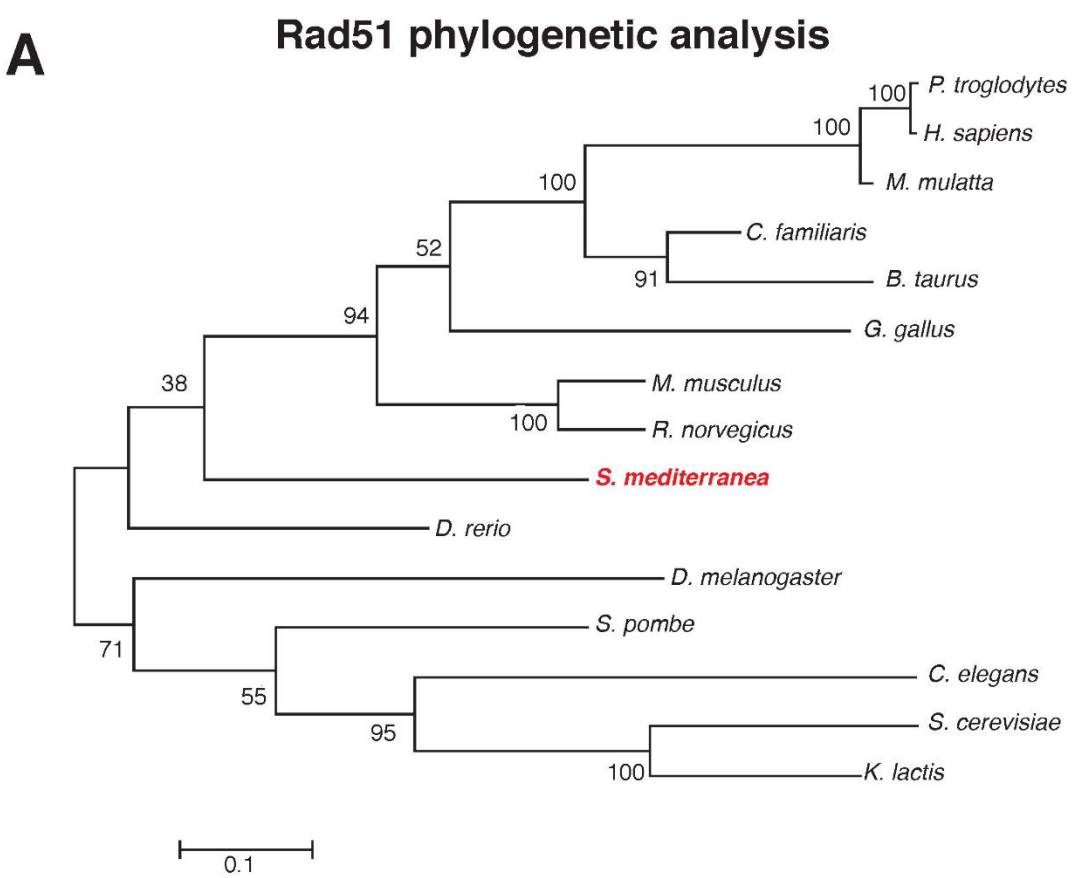

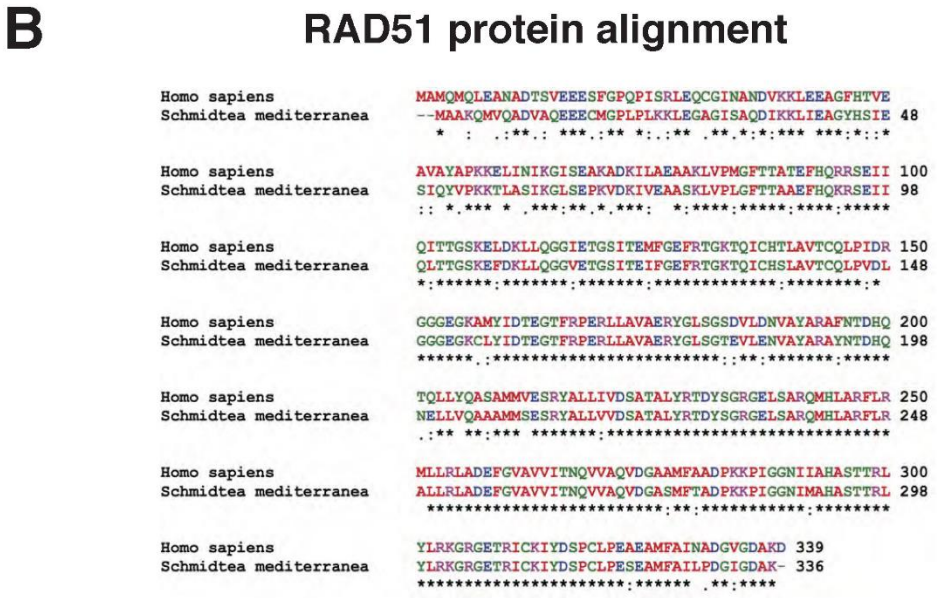

Fig. S2. The *Schmidtea mediterranea* RAD51 protein is evolutionarily and molecularly conserved. (A) Phylogenetic relationship among primates and invertebrates based on the protein sequences of RAD51. Maximum likelihood method was based on the JTT matrix-based model. The percentage of trees in which the associated taxa clustered together is shown next to the branches. The tree is drawn to scale, with branch lengths measured in the number of substitutions per site. Branch support is under 5000 Bootstrap replicas. **(B)** *S. mediterranea* and human RAD51 sequence alignments reveals sequence homology of ~90% with its human counterpart.

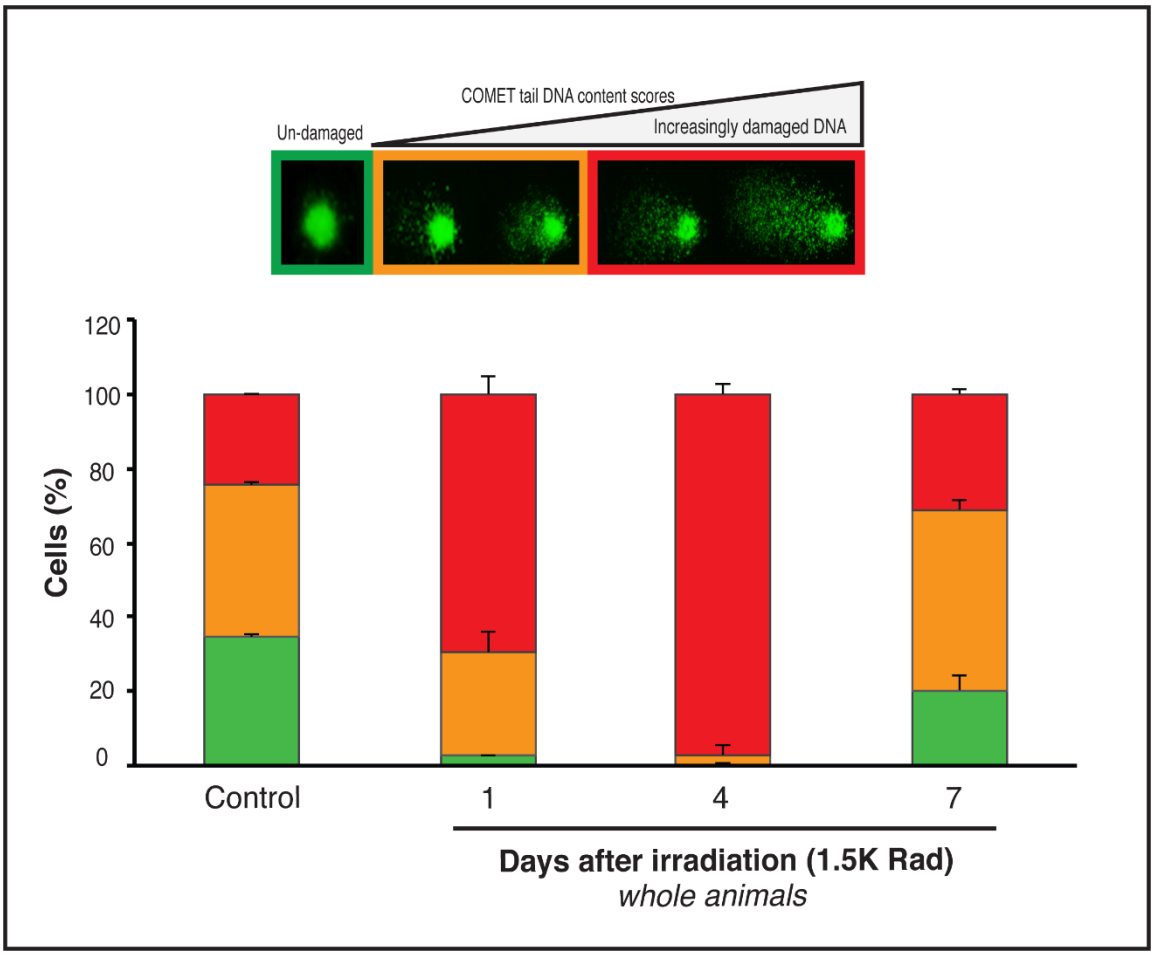

Fig. S3. **The Comet assay detects DNA damage and its repair after sublethal irradiation.** DNA damage in whole organisms assessed by the Comet assay, gel electrophoresis under alkaline conditions. Visual scoring was used to quantify DNA damage, color-coded key at top represents: undamaged (green), moderate damage (orange), and extremely damaged DNA (red) shown. Maximum DNA damage is observed by day 4 post-irradiation, but by day 7 post-irradiation there is considerable less DNA damage. Graph represents mean±s.e.m. of three independent experiments with n=10 animals each. Irradiation consisted of 1,000 rad.

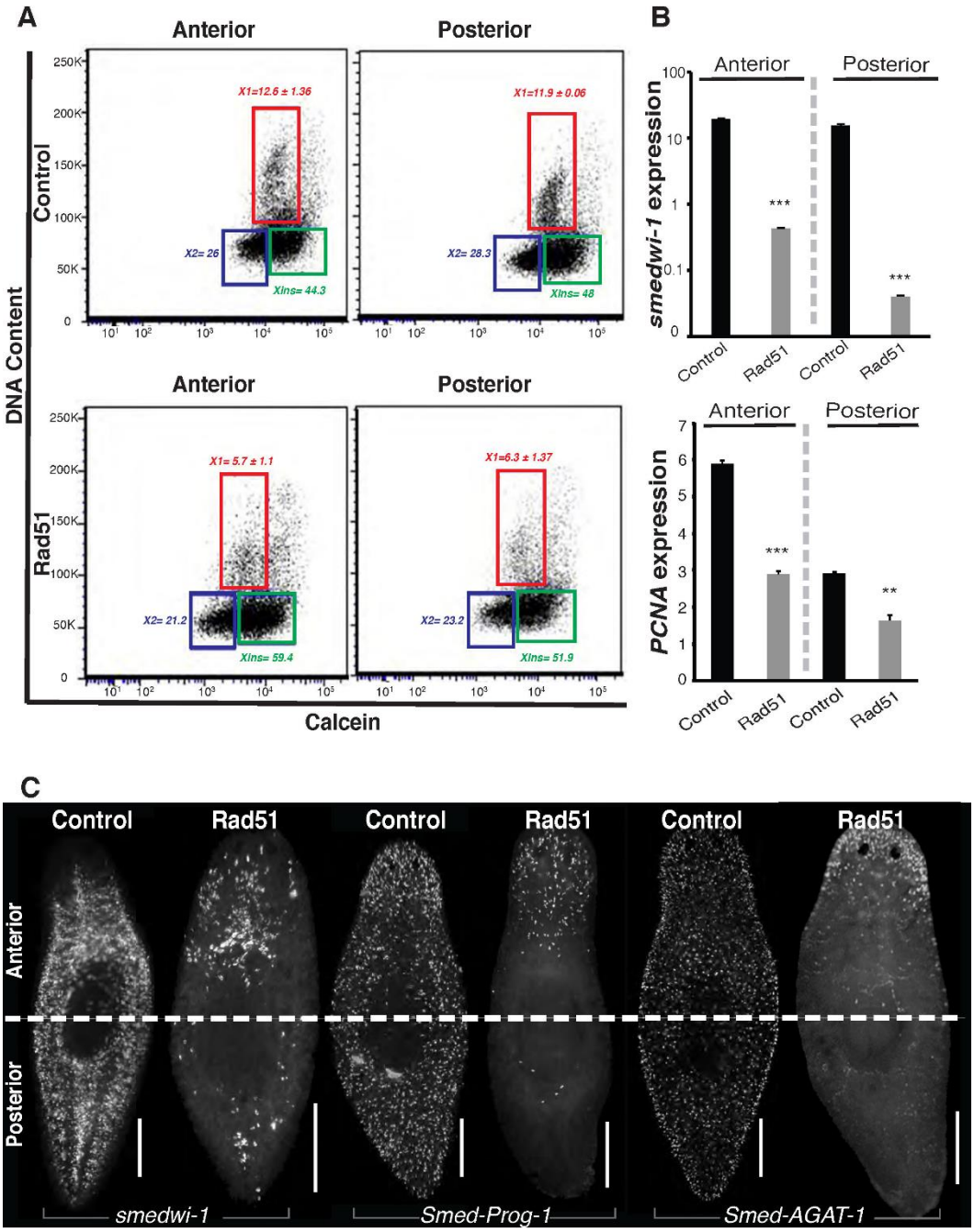

Fig. S4. Systemic Rad51 dysfunction impairs neoblasts and their division progeny. (A) Flow cytometry analysis using Draq5 as the DNA content marker and calcein as the live cell marker shows reduction in the proliferative neoblasts (X1 population) after *Rad51(RNAi)*. The difference in the frequency distribution is statistically significant between different regions of control and *Rad51(RNAi)*, anterior (*P=0.016*) and posterior (*P=0.014*), respectively. For simplicity the extended values for X2 and Xins cells are not shown. **(B)** Gene expression levels of neoblast markers *smedwi-1* and *Smed-PCNA* in anterior and posterior regions of control and *Rad51(RNAi)* animals. **(C)** Whole-mount fluorescent in situ hybridization staining with markers of neoblasts (*smedwi-1*) and their early (*Smed-Prog-1*) and late (*Smed-Agat-1*) progeny. All analyses were performed on intact animals ~30-35 days after first dsRNA injection. All graphs/plots represent mean ± s.e.m. of three or more independent experiments with n=5-10 animals per experiment. Gene expression values represent mean±s.e.m. of triplicates per experiment and at least three biological replicates, each condition was generated by extracting RNA from >20 animals. The internal control is the ubiquitously expressed clone *H.55.12e*. All graphs represents mean±s.e.m. of at least three biological replicates with *n>10* animals per experiment. ****P<0.0001* and ***P=0.004* by Tukey's multiple comparison test. Scale bar, 200 µm.

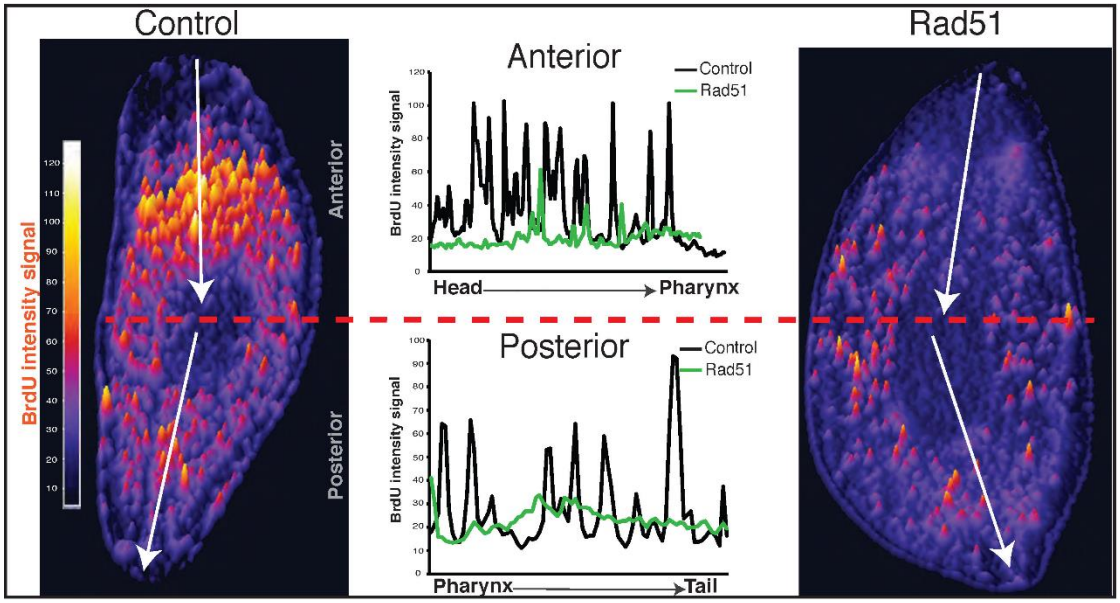

Fig. S5. **The bromodeoxiuridine analog (BrdU) is asymmetrically incorporated along the AP axis.** The intensity of BrdU signal was obtained across the midline of intact (uninjured) controls and *Rad51(RNAi)* animals. Higher levels of the signal are designated with yellow-white and lower levels of intensity are represented by purple color (scale bar on the left). Individual intensity plots are presented for anterior (i.e. head-pharynx, top) and posterior (i.e. pharynx-tail, bottom) region for both control and the experimental group. Intensity of the BrdU signal was calculated with Image J software by drawing a line through the middle of the picture to generate an intensity profile (white arrow). For consistency these are the same pictures found in Figure 3I. However, results show similar tendency in the BrdU intensity across two independent experiments, *n=5* animals each.

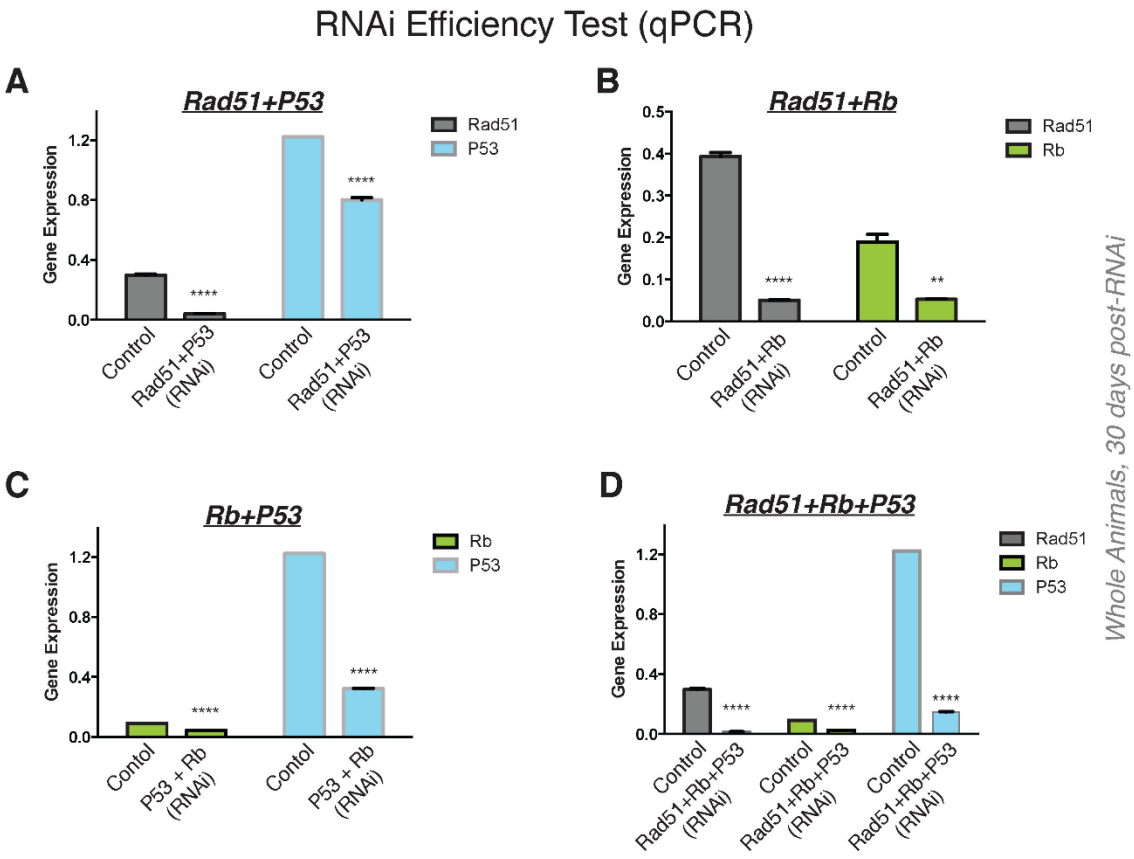

Fig. S6. **Simultaneous downregulation of gene expression with multiple RNAi.** The RNAi efficiency of the RNAi protocols was tested with quantitative PCR (qPCR). (**A-D**) show gene expression for each gene after double and triple downregulating of Rad51, Rb, and p53. RNA was extracted from whole animals subjected to double and triple RNAi after 30 days of the first injection (the particular genes targeted with dsRNA are shown at the top right of each graph). In all cases the RNAi strategy significantly downregulated the expression of the targeted genes ***P<0.001*; *****P<0.0001* by One Way Anova. The average RNAi efficiency is slightly lower in triple RNAi (~80% vs 90% in double RNAi) but there was no difference in the timeline and dynamics of the phenotype at the macroscopic and microscopic levels (not shown). Gene expression values represent mean±s.e.m. of triplicates per experiment and at least three independent experiments, each condition was generated by extracting RNA from >20 animals. The internal control is the ubiquitously expressed clone *H.55.12e*.

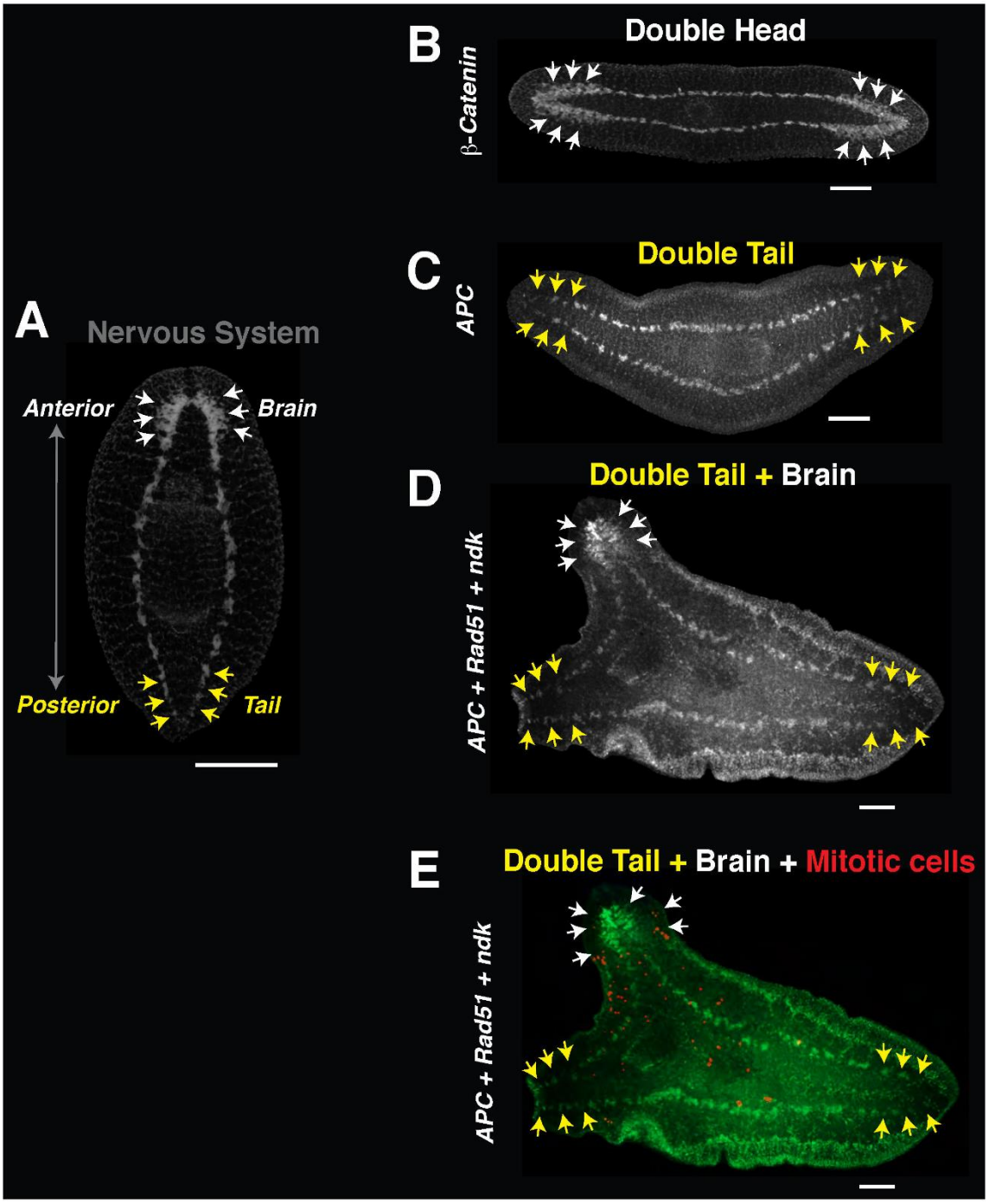

Fig. S7. **Anterior specific nervous tissue modulates cell division in posteriorized animals. (A)** Nervous tissue in planarians is labeled with anti-synapsin antibody (gray signal), which shows accumulation of neurons in the anterior area (cephalic ganglia, for simplicity: brain indicated white arrows) and parallel neural projections that reach the posterior area (ventral nerve cords, VNC, yellow arrows). **(B)** Double headed organism generated by downregulation of *ß-catenin* signaling, note brain tissue at each end of the animal (white arrows). **(C)** RNAi of the *adenomatous polyposis coli (APC)* gene leads to animals that lack brain tissue and display double tail morphology (yellow arrows). **(D)** Triple RNAi involving *APC + Rad51 + nou-darake (ndk)* generates double tail organisms with ectopic brain tissue (white arrows) in which cell division is associated to the proximity of brain tissue (**E**, red signal). Scale bar, 200 µm.

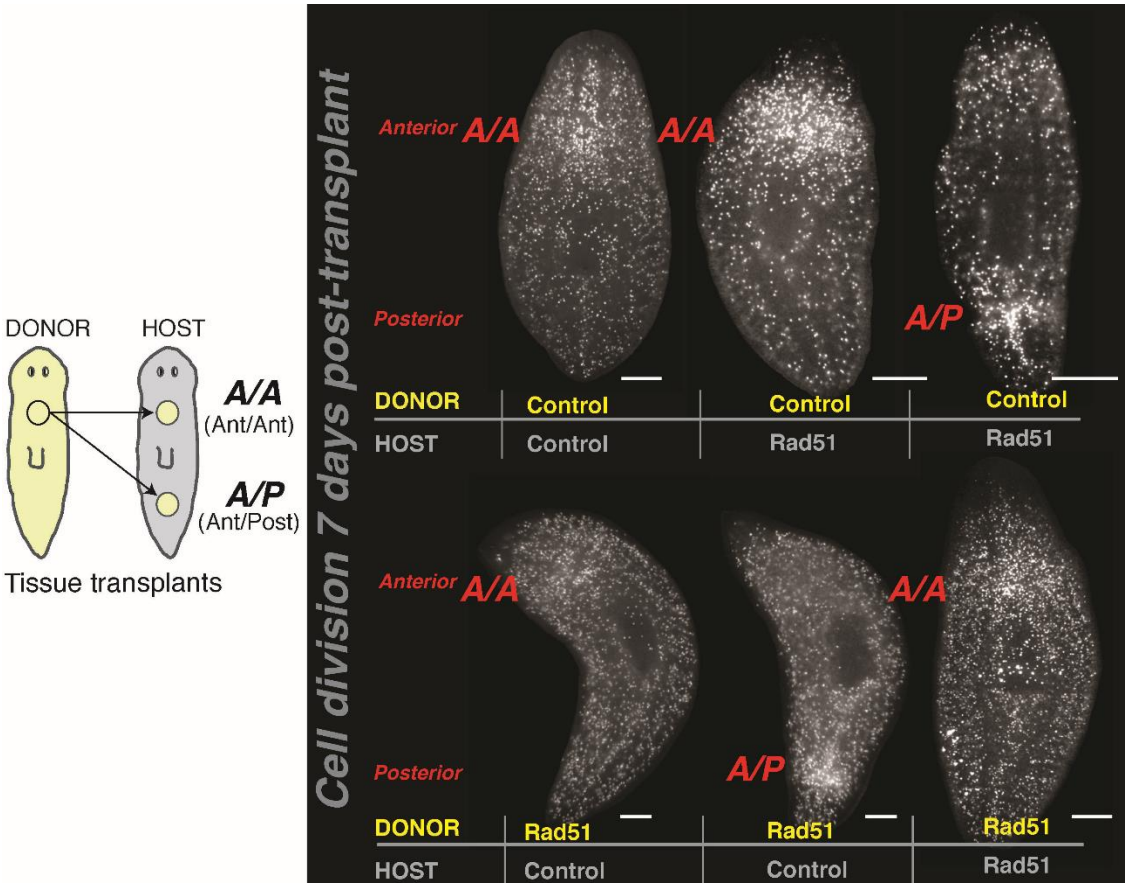

Fig. S8. **Tissue transplants from Rad51 donors lead to hyperproliferation.** Whole-mount immunostaining labeling mitotic activity with the H3P antibody (white dots) one week after tissue transplants were engrafted in either anterior or posterior parts of the animals. Schematic representation of tissue plug transplants from the anterior region of donor animals into host animals (left side), indicated with arrows (*A/A*=anterior to anterior, or *A/P*=anterior to posterior). Donor tissue from control animals was able to re-establish mitotic activity on Rad51 hosts (top row). However, tissue transplanted from Rad51 donors, always led to systemic hyperproliferation (bottom row). All transplants were carried out at 30 days after first dsRNA injection and the images are representatives of two independent experiments, $n>5$ animals each. Scale bar, 200 µm.

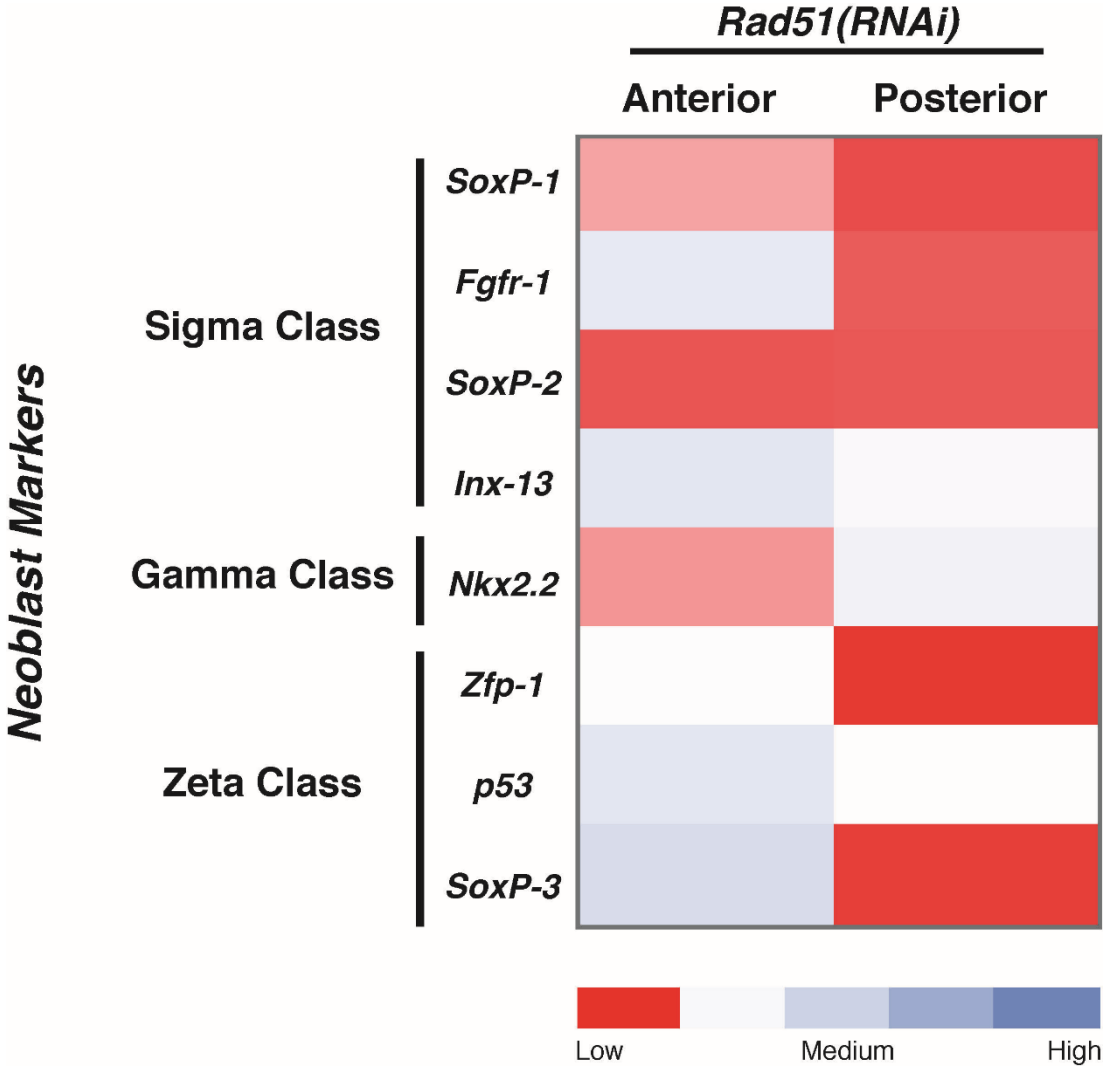

Fig. S9. Rad51 is required for proper expression of neoblast markers. Heat map representation of gene expression levels of neoblast markers in the anterior or posterior regions from the *Rad51(RNAi)* condition with respect to control. Overall, gene expression among different subpopulations of neoblasts (Sigma, Gamma and Zeta) was downregulated but markers of the Zeta class in the anterior region were less impacted than the other neoblast types. The red and blue colors represent fold changes in gene expression levels. Gene expression correspond to the mean of triplicated samples of at least two biological replicates with pooled RNA extraction of >20 animals each. X1 cells serve as the source of RNA in two independent experiments.

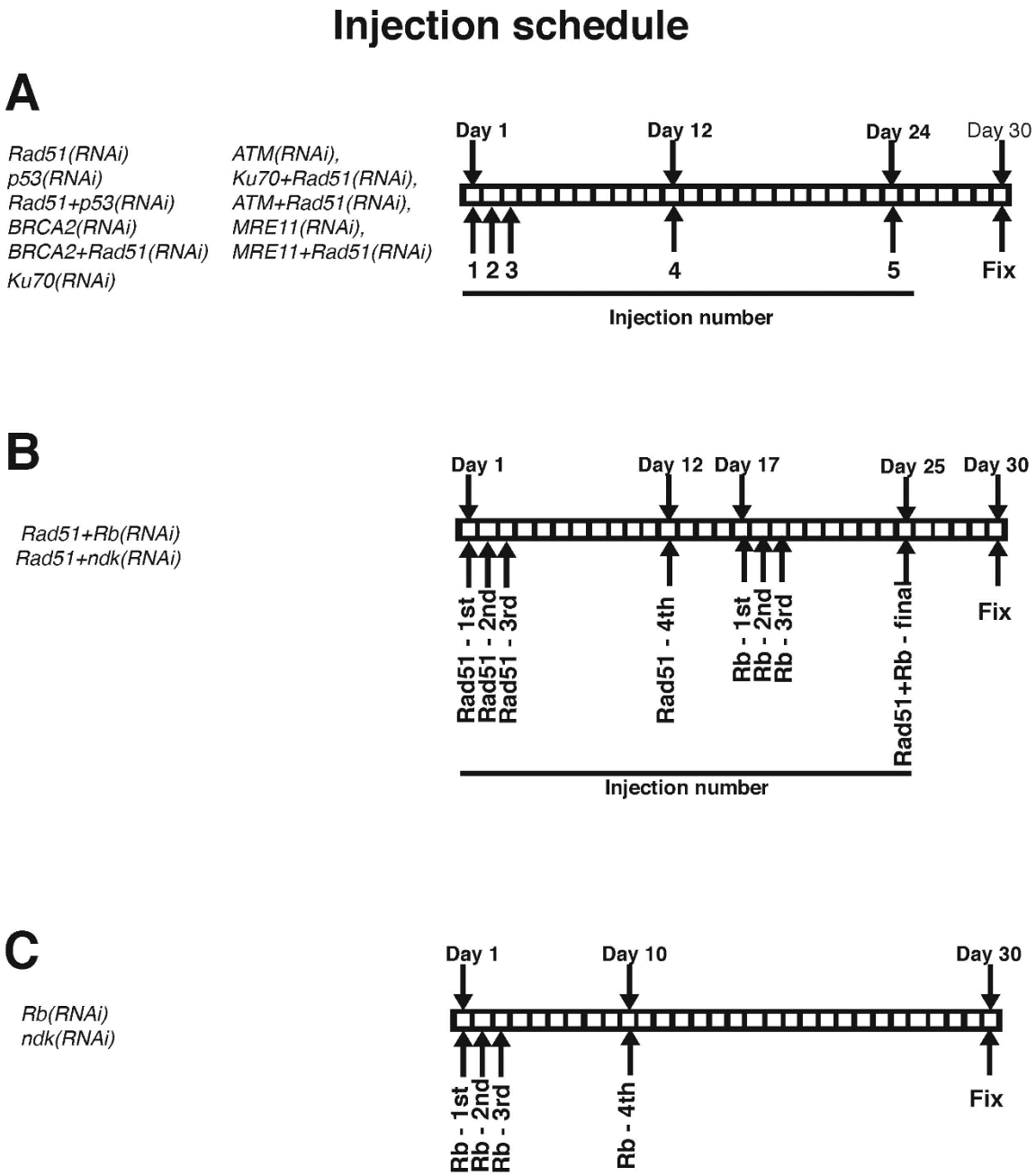

Fig. S10. **dsRNA microinjection schedule. (A, B, C)** Schedule to downregulate genes listed on the left with a total of 4-8 microinjections as illustrated in the lower part of each timeline. Animals were processed 30 days post first injection or at least 4 days after the last injection.

Table S1. List of primers and probes used in this study.

Oligos used for cloning genes and probes		
Name	Forward Primer	Reverse Primer
Rad51	TTTGCAAGGTGGTGTTGAAA	ATCAGCCAACCGTAACAAGG
Ku70	AGGCATGAAATTGGACGAAG	CGACTAGGAGGAGGTGATCG
MRE11	GCATGCAGCGAAGAATTACA	ATCGGATCAATGGCAAAGTC
ATM	GGTTTTGCTTCACGATCCAT	ATCGCAGAAACCAGAGCAGT
Rb	ATGGCGGAGTCAATTTCAAC	GCAATTCGAGAACCTCAAGC
P53	CCTGCTTTTAAATCCGACGA	AAGTGTTTTCCGACCACCTG
BRCA2	ACGATTTACCACCCGAATCA	CGTGAACGTGTCAACAAACC
RPA	GAATCGGACGTCCATGAGAT	GCGGCTGAAATGGAGAAATA
ndk	GAAATTAACGAAGCCCGTCA	TCCCTTTTCACTTTCC
Oligos used for qPCR		
Name	Forward Primer	Reverse Primer
Rad51	ATGTCAGAATCCCGATACGC	ATCAGCCAACCGTAACAAGG
Ku70	TAGTTGGCATTGGGATCCAT	CAGATTTGTGCTGCCTTCAA
MRE11	GCTGGCAACGACTAAGGAAC	CCCGATATATTCCTGGCTGA
ATM	CTGATTGGTCGGCTTTCATT	AGCTAACCAATCCCCCAAAG
Rb	CCACGAGATCCTCCAAATGT	CGTGTGAACATTGGTTTTGC
BRCA2	CAAAGAGACCCTGCTTGAGG	AGCCGGAACACAGTACCATC
UDP	TTCCTACAGCCACTTGAGCGAC	GTCGGTGGTTATTTTGCG
Smedwi-1	TTTATCGTGACGGTGTTGGA	TTGGATTAGCCCCATCTTTG
NB.21.11e	GCAGATGACGTGAAACAAGG	TACTTGATTTGGCGGGAGAC
Agat-1	ACCGATTCCAGTTTCGCTTA	TCAATCGCTCCAAAATCTCA
Cyclin B	TCGGGAAATAGTTCGAATGC	CCAAGGACATCGCAGAAAAT
Soxp-1	TGGTTGGACGTCGCCTTCTT	ACCCATTACCTCCTGAATGGCT
Fgfr-1	CGGCATCCAATAAGTGCGCT	TGTCAGTTTCAGTGGGAACTCCA
Soxp-2	CTTCCCAAGAAGTTTGCTTATTTCTGA	GGCCATTGAATAGTTTCATGATATTTTCCA
Inx13	AAACGGAATCCATTGGTAATAATTCATTCT	GCTGGGTTGAAGGCACTGTT

Nkx2.2	TCGCCAAATTATGCTCAGATTGATCC	CGATTTCTTGTTCACTGGAATTCGGA
Zfp-1	CCCGTGCCTGAACAATTTGACA	CCTCAGCGCATGCCTCTGTA
P53	TGGTTGCATTGCATCGGAACA	GGCCCAGCAATATATTACTTCGGC
Soxp-3	TGTGGTTGGAATTTTTCACTGATTTCT	ACCTGTGCAGACAATTCGAAGA